Analysis of Thickness-Change Induced Local Bending Problems in CFRP-Sandwich Structures

Thomsen, Ole Thybo

Publication date:
1994

Document Version
Publisher's PDF, also known as Version of record

ESTEC Working Paper:
EWP-1787

ANALYSIS OF "THICKNESS-CHANGE" INDUCED LOCAL BENDING PROBLEMS IN CFRP-SANDWICH PANELS

by

Ole Thybo Thomsen
Research Fellow
ESA/ESTEC/YME
Keplerlaan 1, P.O. Box 299
2200 AG Noordwijk ZH, The Netherlands

ESTEC/YME Report No. 2190 - June 1994

Title:

ANALYSIS OF "THICKNESS-CHANGE" INDUCED LOCAL BENDING PROBLEMS IN CFRP-SANDWICH PANELS

Prepared by:

O. T. Thomsen, Research fellow, ESTEC/YME

Summary (extended abstract):

The thickness of face-laminates in CFRP-sandwich panels are often increased locally in order to provide for the load-transfer around highly loaded locations such as joints or inserts. Such thickness-increases are accomplished by adding extra plies to the face-laminates, and a taper is produced by dropping of plies away from the area of localised loading. At all the stations where such thickness drop-offs are made, the local bending stiffness of the face-laminate changes discontinuously, thus inducing severe local bending effects. These local bending effects, in which the face-laminate/core interaction plays an important role, induces interlaminar and bending stresses in the face-laminates, as well as interlaminar stresses in the interface between the core-material and the face-laminates. Thus, the stress concentrations induced in the regions of the dropped plies may initiate delamination, core crushing or direct bending failure of the face-laminates.
The present study introduces a simple method of analysing the thickness-change induced local bending problem in CFRP-sandwich panels. The constituent parts of the model are the base-line laminate of a CFRP-sandwich panel, a dropped sub-laminate, a supporting honeycomb-type core material, and an adhesive/resin-layer interfacing the laminates. The model is based on the assumption that the interaction between the core-material and the face-laminates can be modelled using a two-parameter elastic foundation model, which accounts for the shearing interaction effects. The face-laminates are modelled using classical beam-theory (extendible to plate and shell problems), and the adhesive/resin-layer is modelled using a continuous linear tension/compression and shear spring model. The governing equations are formulated in terms of a set of coupled first order ordinary differential equations, and the resulting "multiple-point" boundary-value problem is solved numerically using the "multi-segment method" of integration.
A few examples have been evaluated using the developed solution procedure, and it has been demonstrated that the local bending response is influenced significantly by the presence of a supporting core material. Thus, *it is shown that the core/face-laminate interaction causes even more severe adhesive/resin layer stress concentrations to occur than is the case for the "unsupported" CFRP-laminate thickness drop-off problem.*
The developed solution procedure has also been used for conducting a series of parametric studies, and it has been shown that three parameters exerts "primary influence" on the local bending problem. These primary parameters are: the ratio of the bending stiffness of the dropped sub-laminate to the base-line laminate; the "characteristic" length of the core/face-laminate interaction; and finally the ratio of the adhesive/resin-layer stiffness to the core transverse stiffness. The overall effect is, that an increase of each of these parameters causes the adhesive/resin stresses, the core stresses, as well as the face-laminate bending stresses to increase significantly.

Keywords:

Local bending, thickness drop-off problem, CFRP-sandwich panels, core/face-laminate interaction, general face/plate/shell-formulation, "multi-segment method" of integration, parametric effects.

LIST OF CONTENTS

ANALYSIS OF "THICKNESS-CHANGE" INDUCED LOCAL BENDING PROBLEMS IN CFRP-SANDWICH PANELS

1. INTRODUCTION

The originating problem for this study was the specific failure mode experienced with a wet filament wound CRFP sandwich structure (Al honeycomb core), representing the central thrust cylinder of a telecommunications satellite designed and manufactured under the ESA-ASTP3 programme. In this programme, a full scale demonstration model thrust cylinder was loaded to failure in a static test with the objective of verifying the strength margin. It was not possible to decide which failure mechanism actually initiated the onset and development of the final failure, but eventually the face-laminates of the thrust cylinder failed completely at a location where the face-laminate thickness changed abruptly. This drop-off in face-thickness was located at the junction between the cylinder central section, and the reinforcing laminates mounted at the ends of the cylinder. These extra layers of CFRP were added to provide the transfer of forces from the thrust cylinder to the end-rings (adhesively bonded to the cylinder). Similar discontinuous thickness-changes of the CFRP-laminates were situated around the areas of the central cylinder where internal fuel tanks were mounted with tank-inserts .
The phenomenon causing failure to occur at the former of the locations described, instead of an overall/local buckling failure somewhere along the midsection of the cylinder (as expected), was most likely local bending induced by the abrupt change of the face bending stiffness caused by change of the face thickness. Thus, in a strict sense, the type of failure experienced by the cylinder was not an instability phenomenon (global/local), but merely a local bending phenomenon.

2. OBJECTIVES

The problem described briefly above, is of more general interest than "just" the design of the satellite thrust cylinders. This is the case, as local bending effects under certain circumstances proves to be the most likely cause of failure, thus adding another possible failure mechanism to the ones usually considered for honey-comb cored CFRP-sandwich panels. The 3 "usual" failure modes being overall buckling, wrinkling and dimpling ("intra-cell" buckling).

The objective of the present study has been defined as the development of a simple analysis-tool capable of describing the local bending phenomenon in terms of the locally induced displacement-, strain- and stress- fields. The analysis tool is intended for conducting a series of parametric studies, where the influence on the local bending state of parameters such as geometrical characteristics, core properties, as well as face properties are included in the investigation.

3. DEFINITION OF THE MECHANICAL MODEL

The problem defined loosely above could be addressed in several different ways, where the most obvious choice might be to conduct a series of FEM-analyses. However, in the present situation, where it is of just as much importance to gain a thorough understanding of the local bending problem and the factors influencing it, as

it is to develop a base of quantitative information, it seems worthwhile to focus the attention to other possible tools.
Moreover, it seems worthwhile to explore the possibility of developing a relatively simple tool, capable of describing the basic mechanics of the problem. This despite the fact, that the level of sophistication of the output data from the simple model may suffer compared to the results obtained from a FEM-analysis using capabilities such as solid modelling, geometrical non-linear analysis, non-linear constitutive models, inclusion of viscous effects, etc.

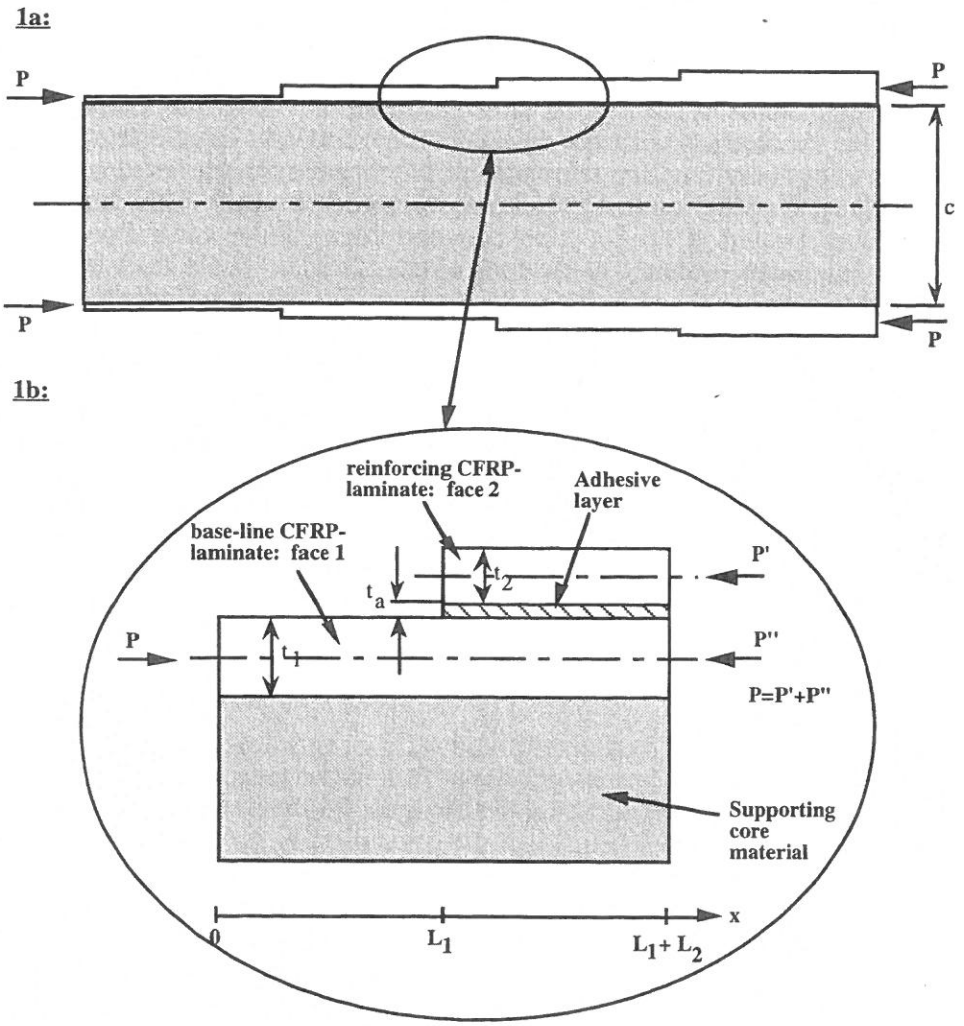

Fig. 1. Definition of mechanical model:
1a: Compression loaded CFRP-sandwich panel with tapered face-laminates.
1b: Local zone around "drop-off" of face laminate thickness.

The mechanical model chosen in this study can be considered as a general beam/ plate/shell model. This is to be understood in the way that the system governing equations for each type of model, or the field equations, can be stated mathematically in the exact same form, thus enabling the use of the same solution procedure independent of the nature of the problem addressed (i.e., a beam-, plate- or shell-problem). This, of course, is a consequence of the fact, that the beam theory (classical Bernoulli-Euler- or Timoshenko-theories) can be considered as a special case of plate

PRINCIPAL NOTATION

Latin symbols:

A_i (i=1,2):	Principal extensional stiffness components of face-laminates 1 and 2; (N/mm).
$(A_{kl})_i$ (k,l=1,3): (i=1,2)	Extensional stiffnesses of face-laminates 1 and 2 obtained from classical laminate theory (CLT). In the present study: $(A_{11})_i=A_i$; (N/mm).
$[\mathbf{A}_{11}(x)]$:	(6,6)-matrix of stiffness coefficients for system of differential equations in region 1.
$[\mathbf{A}_{ij}^*(x)]$ (i,j=1,2):	(6,6)-matrices of stiffness coefficients for system of differential equations in region 2.
b:	Width of face-laminates, b=1 mm in the present study; (mm).
$\{\mathbf{B}_1(x)\}$:	(6,1)-matrix of non-homogeneous load-terms for system of differential equations in region 1.
$\{\mathbf{B}_i^*(x)\}$ (i=1,2):	(6,1)-matrices of non-homogeneous load-terms for system of differential equations in region 1.
c:	Core thickness (mm).
D_i (i=1,2):	Principal bending stiffness components of face-laminates 1 and 2; (Nmm).
$(D_{kl})_i$ (k,l=1,3): (i=1,2)	Bending stiffnesses of face-laminates 1 and 2 obtained from CLT. In the present study: $(D_{11})_i=D_i$; (Nmm).
E_a:	Elastic modulus of adhesive/resin-material; (MPa).
E_a^{eff}:	Effective elastic modulus of adhesive/resin-material, $E_a^{eff}>E_a$; (MPa).
E_c:	Elastic modulus (transverse) of core material; (MPa).
$(E_{kl})_{i,j}$ (k,l=1,2): (i=1,2)	In-plane elastic moduli of the individual laminae of the face-laminates, (j=1,..,n_i); (MPa).
E_0:	Effective transverse elastic modulus of core-material; (MPa).
G_a:	Shear modulus od adhesive/resin-material; (MPa).
$(G_{kl})_{i,j}$ (k,l=1,2): (i=1,2)	In-plane shear moduli of the individual laminae of the face-laminates, (j=1,..,n_i); (MPa).
K_z, K_x:	Transverse and shear foundation moduli of core material; (MPa/mm=N/mm^3).
$F_j(\phi)$ (j=1,2):	"Coefficient functions" for elastic foundation moduli.
L_i (i=1,2):	Lengths of face-laminates in regions 1 and 2; (mm).
L_0:	Characteristic length of core/face-laminate interaction; (mm).
M_i (i=1,2):	Bending moment resultants in face-laminates 1 and 2; (Nmm/mm).
n_i (i=1,2):	Number of laminae in face-laminates 1 and 2.
N_i (i=1,2):	Normal stress resultants in face-laminate 1 and 2; (N/mm).
P:	Compressive in-plane load; (N/mm).
Q_i (i=1,2):	Transverse shear stress resultants in face-laminates 1 and 2; (N/mm).
s:	Honeycomb-core cell-size: largest circle-diameter which can be inscribed in the honeycomb-cells; (mm).
t_a:	Thickness of adhesive/resin-layer interfacing face-laminates 1 and 2; (mm)
t_i (i=1,2):	Thicknesses of face-laminates 1 and 2; (mm).
$[\mathbf{T}_0]$:	Non-singular (6,6) transformation matrix specifying the boundary conditions at x=0.
$[\mathbf{T}_i]$:	Non-singular (12,12) transformation matrices.
u_i (i=1,2):	Longitudinal displacements of face-laminates 1 and 2; (mm).
u_{0i} (i=1,2):	Longitudinal displacements of mid-surfaces of face-laminates 1 and 2; (mm).

$\{\mathbf{U}_0\}$:		(6,1)-matrix containing the fundamental variables at x=0.
$\{\mathbf{U}_i\}$:	(i=1,2)	(12,1)-matrices containing the fundamental variables at x=L_1 and x=L_1+L_2.
w_i	(i=1,2):	Lateral displacements of face-laminates 1 and 2; (mm).
x:		Longitudinal coordinate; (mm).
$\{y_i(x)\}$	(i=1,2):	(6,1)-matrix of fundamental variables for face-laminates 1 and 2; $\{y_i(x)\}=\{u_i(x), w_i(x), \beta_i(x), N_i(x), M_i(x), Q_i(x)\}$.
z:		Transverse coordinate; (mm).
$z_{i,j}$	(i=1,2) (j=1,..,n_i)	Transverse coordinate within each lamina of the face-laminates; (mm).

Greek symbols:

β_i	(i=1,2):	Rotation of normal to midsurface of face-laminates 1 and 2; (rad).
ϕ:		Non-dimensional geometric coefficient (foundation model).
γ:		Non-dimensional coefficient (foundation model); (γ=1.5).
λ:		Wave-length of elastic response ($\lambda = 2\pi L_0$); (mm).
Λ:		Ratio of adhesive/resin-layer stiffness to core transverse stiffness.
ν_a:		Poisson's ration of adhesive/resin-material.
ν_c:		Poisson's (transverse) ratio of core-material.
ν_0:		Effective Poisson's ratio of core-material.
$(\nu_{kl})_{i,j}$	(k,l=1,2): (i=1,2)	In-plane Poisson's ratios of the individual laminae of the face-laminates; j=1,..,n_i.
σ_a:		Adhesive/resin-layer transverse normal stress; (MPa)
σ_c:		Core transverse normal stress (interface between core and face-laminates); (MPa).
$\sigma_{i,j}$	(i=1,2): (j=1,..,n_i)	Bending stress components in laminae of face-laminates; (MPa).
σ_N:		Nominal stress, $\sigma_N=N_1(x=0)/t_1$; (MPa)
τ_a:		Adhesive/resin-layer shear stress; (MPa).
τ_c:		Core shear stress (interface between core and face-laminates); (MPa).

Superscripts:

( )':	Differentiation with respect to x-coordinate: ( )'=d( )/dx.

theory (Kirchhoff- or Mindlin-theories), which again can be considered as a special case of general shell theory (Love-Kirchhoff- or "higher order"- shear theories).
The problem considered is illustrated in Fig. 1a, which shows a part of a honeycomb-cored CFRP-sandwich panel loaded in compression. The thickness of the face-laminates varies stepwise over the length of the sandwich panel. The local area around such a thickness drop-off is shown schematically in Fig. 1b, which also defines the mechanical model used for describing the local bending problem.
The model shown in Fig. 1b considers the face of the sandwich-panel (being modelled as a beam, a plate in cylindrical bending, or a circular cylinder) as elastically supported on the core material of the sandwich panel. The face is subjected to the compressive load P. The thickness of the face changes from t_1 to $t_1+t_a+t_2$ over the length of the considered face section, where t_a is the thickness of the adhesive layer (or resin-"rich" layer for co-cured face-laminates) between the two laminates.

4. *DERIVATION OF SYSTEM GOVERNING EQUATIONS*

The system of governing equations are set up for the simplest possible case, i.e. where the faces are considered as laminated beams or plates in cylindrical bending. If the need for a more general shell formulation appears, however, the formulation can be extended without any principal difficulties. In the most general form, the model will be able to account for any rotationally symmetric shell configuration, with generally orthotropic material properties (i.e., arbitrary stacking sequences and principal material directions), as well as arbitrary boundary and load conditions (i.e., also non-axisymmetric conditions).

In the beam-approach, the formulation of the governing equations is based on the ordinary "Bernoulli-Euler" theory: i.e., it is assumed that normals to the undeformed neutral-axis of the face-laminates remains straight, normal and inextensional during deformation, so that transverse normal and shearing strains may be neglected in deriving the face kinematic relations.

Referring to Fig. 1b, it is observed that the system governing equations has to be set up in the two adjoining regions:

1. Region 1: $0 \le x \le L_1$.
2. Region 2: $L_1 \le x \le L_1 + L_2$.

The face kinematic relations are given by (valid in both regions):

$$(1) \qquad u_i = u_{0i} + z\beta_i, \quad \beta_i = -w_i' \quad (i = 1,2)$$

where u_i is the longitudinal displacement component, u_{0i} is the longitudinal displacement component of the face-laminate neutral-axis ("membrane"-contribution), β_i is the rotation of the face-laminate normal, w_i is the lateral deflection of the face-laminate, ( )' denotes differentiation with respect to the longitudinal coordinate x, and i=1, 2 corresponds to face-laminates 1 and 2, respectively (see Fig. 1b).

Referring to Fig. 2, the equilibrium equations in region 1 can be written as:

$$
\begin{aligned}
N_1' &= \tau_c, \\
Q_1' &= \sigma_c, \\
M_1' &= Q_1 - \tau_c \frac{t_1}{2}
\end{aligned}
\qquad (2)
$$

where N_1, Q_1, M_1 are the normal stress, transverse shear, and bending moment resultants in face-laminate 1. σ_c is the foundation (i.e., core) transverse normal stress component, and τ_c is the foundation shear stress component.

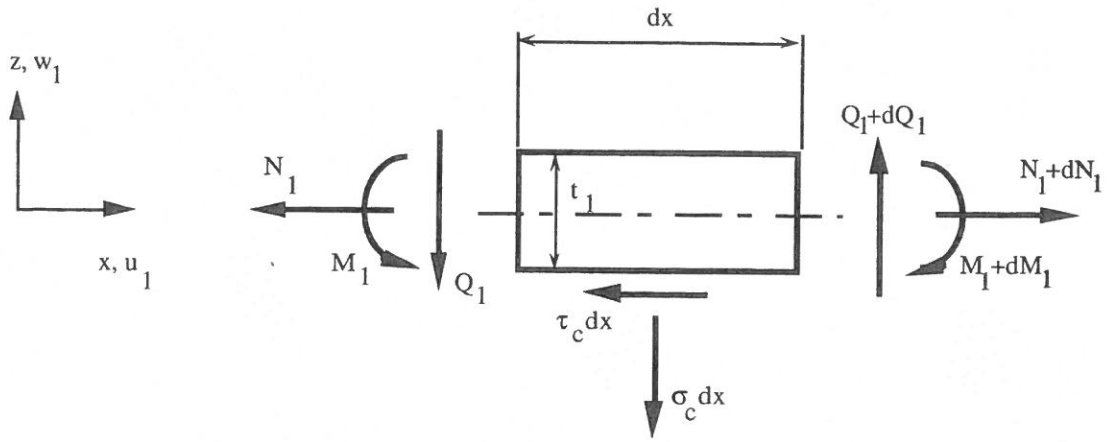

Fig. 2. Equilibrium element of face-laminate 1 in region 1; $0 \le x \le L_1$.

The interaction between the supporting core material and the CFRP-face laminate is modelled using a "two-parameter" elastic foundation model, which takes into account the shear interaction effects between the core and face-laminates. The elastic response of the core material is suggested expressed using the following expressions (according to ref. 1), relating the face-laminate deflections u_1 (only bending contribution) and w_1 to the core stress components σ_c, τ_c:

$$
\sigma_z = K_z w_1, \quad \tau_c = K_x \underbrace{\left\{ u_1(x, -\frac{t_1}{2}) \right\}}_{\text{BENDING CONTRIBUTION}} = -K_x \frac{t_1}{2} \beta_1 \qquad (3)
$$

where K_z and K_x are the elastic foundation moduli of the core material. According to refs.1 and 2, appropriate expressions for K_z, K_x can be given as (in slightly modified form):

$$
\begin{aligned}
&K_z = \frac{E_0 \gamma}{b(1-\nu_0^2)} F_1(\phi), \quad K_x = \frac{E_0 b}{4 t^* c \gamma (1+\nu_0)} F_2(\phi), \\
&F_1(\phi) = \frac{\sinh(\phi)\cosh(\phi)+\phi}{\sinh^2(\phi)}, \quad F_2(\phi) = \frac{\sinh(\phi)\cosh(\phi)-\phi}{\sinh^2(\phi)}, \\
&\phi = \frac{2\gamma c}{b}, \quad E_0 = \frac{E_c}{1-\nu_c^2}, \quad \nu_0 = \frac{\nu_c}{1-\nu_c}, \quad \gamma = 1.5, \\
&b = 1.0\,mm \text{ ("unit width")}, \quad t^* = \begin{cases} t_1 & \text{in region 1} \\ t_1 + t_a + t_2 & \text{in region 2} \end{cases}
\end{aligned}
\qquad (4)
$$

where c is the core height, E_c is the transverse elastic modulus, and ν_c is the Poisson's ratio of the core material.
By combining equations (1)-(3) followed by some rearrangement the governing equations in region 1 ($0 \le x \le L_1$) can be written in the form:

$$u_{01}' = \frac{N_1}{A_1}, \quad w_1' = -\beta_1, \quad \beta_1' = \frac{M_1}{D_1},$$

$$N_1' = -\beta_1 \frac{K_x t_1}{2}, \quad M_1' = \beta_1 \frac{K_x t_1^2}{4} + Q_1, \tag{5}$$

$$Q_1' = K_z w_1$$

where A_1, D_1 are the extensional and bending stiffnesses of face-laminate 1. Equations (5) constitutes a set of 6 linear coupled first-order ordinary differential equations.

The system of governing equations in region 2 (see Fig. 1b), are set up in the same way as in region 1, the only difference being that the governing equations have to be specified for both face-laminates (1 and 2).

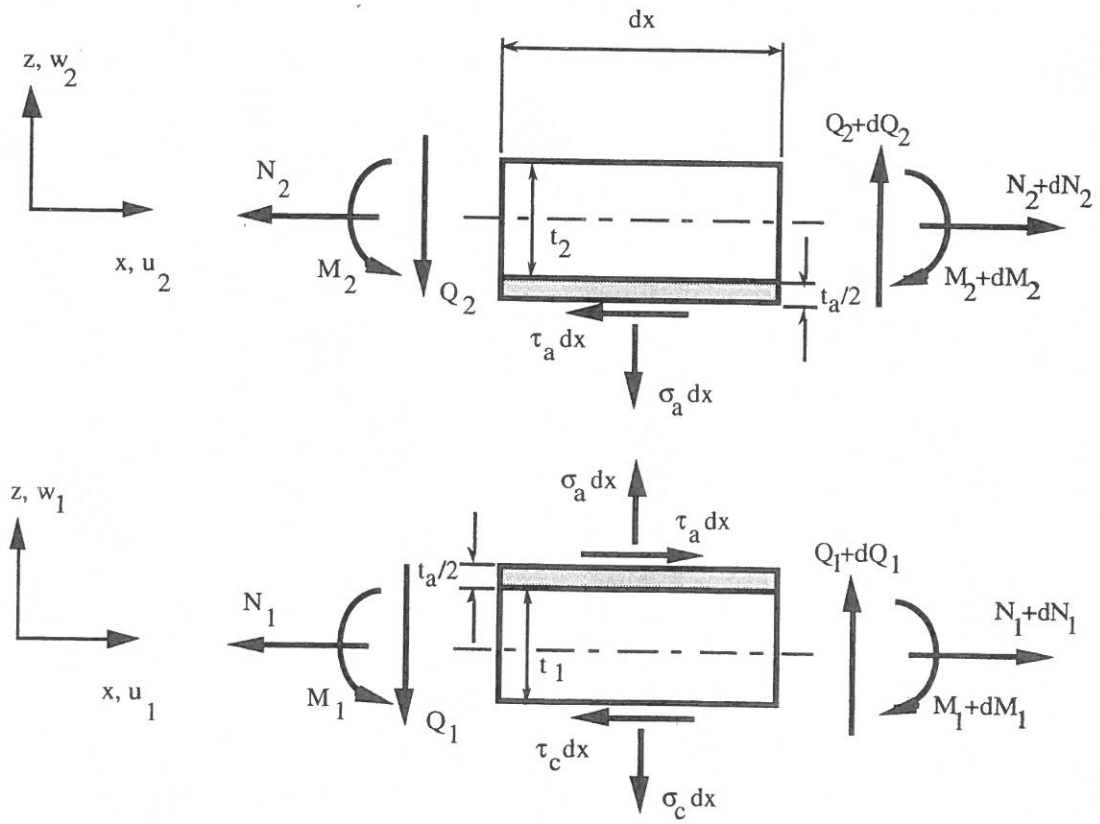

Fig. 3. Equilibrium elements of face-laminates 1 and 2 in region 2; $L_1 \le x \le L_1+L_2$.

Referring to Fig. 3, the equilibrium equations in region 2 can be specified as:

$$(6)\qquad \textit{Region 1:}\ \begin{cases} N_1' = \tau_c - \tau_a, \\ Q_1' = \sigma_c - \sigma_a, \\ M_1' = Q_1 - \tau_c \frac{t_1}{2} - \tau_a \frac{t_1 + t_a}{2} \end{cases} \qquad \textit{Region 2:}\ \begin{cases} N_2' = \tau_a, \\ Q_2' = \sigma_a, \\ M_2' = Q_2 - \tau_a \frac{t_2 + t_a}{2} \end{cases}$$

σ_a, τ_a are the adhesive layer transverse normal (peel- or cleavage stress) and shear stress components. The coupling between the two face-laminates is established through the constitutive relations of the adhesive/resin layer, which is assumed to be homogeneous, isotropic and linear elastic. According to ref. 3, the adhesive layer constitutive equations are suggested in the form:

$$(7)\qquad \sigma_a = \frac{E_a^{eff}}{t_a}\{w_2 - w_1\}, \quad \tau_a = \frac{G_a}{t_a}\left\{u_{02} - \frac{t_2}{2}\beta_2 - u_{01} - \frac{t_1}{2}\beta_1\right\}$$

where G_a is the shear modulus, and E_a^{eff} is the effective elastic modulus of the adhesive material. E_a^{eff} is somewhat larger than E_a (adhesive elastic modulus), and is introduced in order to account for the prevented straining of the adhesive layer[1].

---

1 E_a^{eff} can be found from the elastic stress-strain relationship for the adhesive:

$$(i)\qquad \sigma_{za} = \frac{E_a}{1+\nu_a}\left\{\varepsilon_{za} + \frac{\nu_a}{1-2\nu_a}\left(\varepsilon_{xa} + \varepsilon_{ya} + \varepsilon_{za}\right)\right\}$$

Because of the compability of strains across the interface between the face-laminates and the adhesive layer, ε_{xa} and ε_{ya} in the adhesive layer must be equal in magnitude to the adherend strains ε_{xi}, ε_{yi} (i=1,2) on the interfaces, whereas the transverse adhesive layer normal strain ε_{za}, which is given by (ε_{za} is assumed constant over the adhesive thickness):

$$(ii)\qquad \varepsilon_{za} = \frac{w_2 - w_1}{t_a}$$

can be much larger. Thus, the following statement is true:

$$(iii)\qquad |\varepsilon_{za}| >> (\varepsilon_{xa}, \varepsilon_{ya})$$

If ε_{xa} and ε_{ya} are neglected in comparison with ε_{za}, eq. (i) can reduced to:

$$(iv)\qquad \sigma_{za} = \sigma_a \approx \frac{E_a}{1+\nu_a}\left\{\varepsilon_{za} + \frac{\nu_a}{1-2\nu_a}\varepsilon_{za}\right\} = E_a^{\,eff}\varepsilon_{za} \quad \Leftrightarrow$$
$$E_a^{\,eff} = E_a \frac{(1-\nu_a)}{(1-2\nu_a)(1+\nu_a)}$$

making E_a^{eff} somewhat larger than E_a ($E_a^{eff} > E_a$ for physically realistic values of ν_a: $0.25 \le \nu_a \le 0.45$).

Combination of equations (1), (3) and (7), yields the set of governing equations in region 2:

Face 1:

$$
\text{(8a)}\quad
\begin{cases}
u_{01}' = \dfrac{N_1}{A_1}, \quad w_1' = -\beta_1, \quad \beta_1' = \dfrac{M_1}{D_1}, \\
N_1' = u_{01}\dfrac{G_a}{t_a} + \beta_1\left[\dfrac{G_a t_1}{2t_a} - \dfrac{K_x t_1}{2}\right] - u_{02}\dfrac{G_a}{t_a} + \beta_2\dfrac{G_a t_2}{2t_a}, \\
M_1' = u_{01}\dfrac{G_a(t_1+t_a)}{2t_a} + \beta_1\left[\dfrac{G_a(t_1+t_a)t_1}{4t_a} + \dfrac{K_x t_1^{\,2}}{4}\right] - u_{02}\dfrac{G_a(t_1+t_a)}{2t_a} \\
\qquad + \beta_2\dfrac{G_a(t_1+t_a)t_2}{4t_a} + Q_1, \\
Q_1' = w_1\left[K_z + \dfrac{E_a^{\,eff}}{t_a}\right] - w_2\dfrac{E_a^{\,eff}}{t_a}
\end{cases}
$$

Face 2:

$$
\text{(8b)}\quad
\begin{cases}
u_{02}' = \dfrac{N_2}{A_2}, \quad w_2' = -\beta_2, \quad \beta_2' = \dfrac{M_2}{D_2}, \\
N_2' = -u_{01}\dfrac{G_a}{t_a} - \beta_1\dfrac{G_a t_1}{2t_a} + u_{02}\dfrac{G_a}{t_a} - \beta_2\dfrac{G_a t_2}{2t_a}, \\
M_2' = u_{01}\dfrac{G_a(t_2+t_a)}{2t_a} + \beta_1\dfrac{G_a(t_2+t_a)t_1}{4t_a} - u_{02}\dfrac{G_a(t_2+t_a)}{2t_a} + \beta_2\dfrac{G_a(t_2+t_a)t_2}{4t_a} + Q_2, \\
Q_2' = -w_1\dfrac{E_a^{\,eff}}{t_a} + w_2\dfrac{E_a^{\,eff}}{t_a}
\end{cases}
$$

where A_2, D_2 are the extensional and bending stiffnesses of face-laminate 2. Equations (8a-b) constitutes a set of 12 coupled linear first order ordinary differential equations.

Equations (5) and (8a-b) represents the set of governing equations in regions 1 and 2, and the only thing still needed is the formulation of the boundary conditions. With reference to Fig. 1b, the boundary conditions are suggested as follows:

$$
\text{(9)}\quad x = 0: \quad
\begin{cases}
w_1 = 0 \\
N_1 = -P \quad \text{("simple support" condition),} \\
M_1 = 0
\end{cases}
$$

$$
\text{(10)}\quad x = L_1: \quad
\begin{cases}
\textit{Face 1:} & \begin{cases} \text{"continuity" of solution across junction} \\ \text{between regions 1 and 2,} \end{cases} \\
\textit{Face 2:} & \begin{cases} N_2 = 0 \\ M_2 = 0 \quad \text{("free edge" condition),} \\ Q_2 = 0 \end{cases}
\end{cases}
$$

$$(11)\qquad x = L_1 + L_2: \begin{cases} \textit{Face 1:} & \begin{cases} u_{01} = 0 \\ \beta_1 = 0 \\ Q_1 = 0 \end{cases} \quad \text{("symmetry" condition),} \\ \textit{Face 2:} & \begin{cases} u_{02} = 0 \\ \beta_2 = 0 \\ Q_2 = 0 \end{cases} \quad \text{("symmetry" condition)} \end{cases}$$

The statement of the boundary conditions at the ends of the modelled "drop-off", i.e., the assumption of simple support at x=0 and "symmetry" conditions at $x=L_1+L_2$, of course contains an element of arbitrariness, as the "real" boundary conditions for a thickness "drop-off" in the middle of a sandwich panel are likely to be more complicated. However, given that the considered length of the thickness "drop-off" section (L_1+L_2) is sufficiently large, the actual boundary conditions imposed at x=0 and $x=L_1+L_2$ are not very important. This is due to the fact, that the local bending effects only extends a very short distance to each side of the discontinuous thickness change (as will be demonstrated later).

5. *SOLUTION : "THE MULTI-SEGMENT METHOD OF INTEGRATION"*

The set of governing equations (5), (8a-b) together with the statement of the boundary conditions, given by equations (9)-(11), constitutes a "multiple-point" boundary value problem, which can be expressed in the following general form:

Governing equations:

$$(12)\qquad \begin{aligned} &0 \le x \le L_1: && \{y_1(x)\}' = [\mathbf{A}_{11}(x)]\{y_1(x)\} + \{\mathbf{B}_1(x)\} \\ &L_1 \le x \le L_1 + L_2: && \begin{Bmatrix} \{y_1(x)\} \\ \{y_2(x)\} \end{Bmatrix}' = \begin{bmatrix} [\mathbf{A}^*_{11}(x)] & [\mathbf{A}^*_{12}(x)] \\ [\mathbf{A}^*_{21}(x)] & [\mathbf{A}^*_{22}(x)] \end{bmatrix} \begin{Bmatrix} \{y_1(x)\} \\ \{y_2(x)\} \end{Bmatrix} + \begin{Bmatrix} \{\mathbf{B}^*_1(x)\} \\ \{\mathbf{B}^*_2(x)\} \end{Bmatrix} \end{aligned}$$

$$(13)\qquad \textit{Boundary conditions:} \begin{cases} x = 0: & [\boldsymbol{T}_0]\{y_1(0)\} = \{\boldsymbol{U}_0\}, \\ x = L_1: & [\boldsymbol{T}_1]\begin{Bmatrix} \{y_1(L_1)\} \\ \{y_2(L_1)\} \end{Bmatrix} = \{\boldsymbol{U}_1\}, \\ x = L_1 + L_2: & [\boldsymbol{T}_2]\begin{Bmatrix} \{y_1(L_1 + L_2)\} \\ \{y_2(L_1 + L_2)\} \end{Bmatrix} = \{\boldsymbol{U}_2\} \end{cases}$$

In equations (12), $\{y_i(x)\} = \{u_{0i}(x), w_i(x), \beta_i(x), N_i(x), M_i(x), Q_i(x)\}$ $(i=1,2)$ are the (6,1) matrices (vectors) of so-called fundamental variables, $[\mathbf{A}_{11}(x)]$, $[\mathbf{A}_{ij}{}^*(x)]$ (i,j=1,2) are (6,6) matrices of stiffness coefficients; and $\{\mathbf{B}_1(x)\}$, $\{\mathbf{B}_i{}^*(x))\}$ (i=1,2) are vectors of non-homogeneous load terms (zero in this problem as no external surface loads are specified).
In equations (13), $[\boldsymbol{T}_0]$ is a non-singular (6,6) transformation matrix, and $[\boldsymbol{T}_1]$, $[\boldsymbol{T}_2]$ are non-singular (12,12) transformation matrices. $\{\boldsymbol{U}_0\}$ is a (6,1) matrix containing the fundamental variables at x=0, and $\{\boldsymbol{U}_1\}$, $\{\boldsymbol{U}_2\}$ are (12,1) matrices containing the

fundamental variables at $x=L_1$ and $x=L_1+L_2$. It should be emphasised here, that the form of the equations (13) does not involve any restrictions on the boundary conditions, and that any natural boundary conditions may be stated in this form.

Considering the "multiple-point" boundary value problem thus stated (eqs. (12), (13)), it appears that no general closed-form solutions are obtainable. Thus, a numerical solution procedure has to be developed. Such a numerical solution procedure can be developed by following two possible approaches:

1. the finite difference method,
2. the direct integration method ("multi-segment method of integration").

The latter offers some advantages compared to the former, where the most significant ones in this context are:

- It can be applied conveniently to systems of first order equations.
- It can be applied equally well to beam, plate and shell problems.
- It is especially well suited for solving "multiple-point" boundary value problems.

Thus, the multi-segment method of integration will be used for the present study. Without going into details, the method is based on a transformation of the original "multiple-point" boundary value problem into a series of initial value problems. Referring to Fig. 4, the problem consisting of the elastically supported face elements is divided into a finite number of segments ($N_1 + N_2$, usually 10-25 elements), and the solution within each segment can be accomplished by means of any of the standard methods of direct integration (Runge-Kutta, or Predictor-Corrector methods). Continuity of al the solution vectors $\{y_i(x)\}$ (containing the fundamental variables of the problem) at the boundaries ($x=0$, L_1, L_1+L_2), and at the separation points between the segments, is ensured by formulating and solving a set of linear algebraic equations. For more detailed information about the multi-segment method of integration, the reader is referred to refs. 4 and 5.

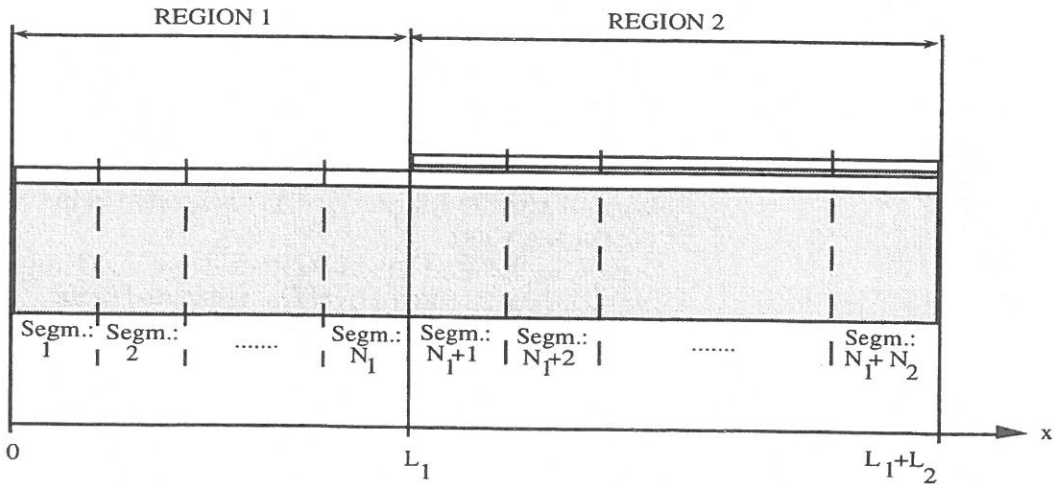

Fig. 4. CFRP-sandwich face thickness "drop-off" problem divided into $N_1 + N_2$ segments.

The implementation of the developed solution procedure, has been carried out using the mathematical software-package MATLAB® version 4.1, which supplies a technical computing environment for numeric computation and visualisation. A UNIX-version of MATLAB®, installed on a HP workstation, was used for the development of the described solution procedure as well as for the conduction of a parametric study (the details of which will be given later). The part of the solution involving direct integration, is based on a MATLAB®-routine using an "adaptive step-size" 4th and 5th order Runge-Kutta-Fehlberg method.
No further details about the MATLAB®-implementation will be given, except that it should be stated that the solution procedure was very easy to implement in the MATLAB® environment, and, moreover, that the resulting MATLAB®-program is very "cost-effective" in terms of computer power needed (run-time is usually 10-30 CPU seconds on the HP-workstation).
The developed MATLAB® source-code is given in appendices 1-20 of this report.

6. *EXAMPLES*

To demonstrate the applicability of the developed solution procedure, as well as to illustrate the basic mechanical characteristics of the thickness "drop-off" problem in CFRP-faced sandwich panels, a couple of examples will be given.

6.1 *Example 1: "sandwich face-laminate thickness drop-off"*

The first example given represents a thickness "drop-off" of a symmetric honeycomb-cored sandwich panel with CFRP-faces. The elastic and geometrical properties of the sandwich panel are assumed to be as follows:

Face 1(base-line laminate):
5-ply laminate made of UD-prepregs: HTS carbon fibres in an epoxy resin system with curing temperature of 120 °C (code 92). The ply-thickness is 0.05 mm corresponding to 60% fibre volume (as specified for a CFRP-sandwich thrust-cylinder in ref. 6):

Stacking sequence:	symmetric lay-up;$[\pm 25^\circ, 0^\circ, \mp 25^\circ]$.
Laminate thickness:	t_1=0.25 mm.
Laminate properties:	A_{11}=22.0 kN/mm, A_{12}=3.5 kN/mm, A_{22}=2.6 kN/mm, A_{66}=4.0 kN/mm (only A_{11}="A_1" is needed in the present analysis). D_{11}=106.0 Nmm, D_{12}=22.0 Nmm, D_{22}=15.0 Nmm, D_{66}=25.0 Nmm (only D_{11}="D_1" is needed in the present analysis).
Length, region 1:	L_1=10.0 mm.

Face 2 (reinforcing laminate):
2-ply laminate made from the same HTS carbon fibre/epoxy resin system as face-laminate 1:

Stacking sequence:	non-symmetric lay-up;$[\pm 45^\circ]$.
Laminate thickness:	t_2=0.10 mm.
Laminate properties:	A_{11}=3.6 kN/mm, A_{12}=2.8 kN/mm, A_{22}=3.6 kN/mm, A_{66}=2.8 kN/mm (as before, only A_{11}="A_2" is needed in the present analysis). D_{11}=3.0 Nmm, D_{12}=2.3 Nmm, D_{22}=3.0 Nmm,

D_{66}=2.3 Nmm (as before, only D_{11}="D_2" is needed in the present analysis).
The existence of non-zero "B-matrix" elements (caused by the non-symmetric lay-up) is ignored.

Length, region 2: L_2=10.0 mm.

Core material:

HEXCEL Al-Honeycomb: 3/16"-5056-0.0007":

Cell-size: s=3/16"=4.8 mm,

Core thickness: c=10.0 mm,

Elastic properties: E_c=310.0 MPa, ν_c=0.3 ("out-of-plane" properties).

Adhesive material:

The adhesive layer is assumed to have the same characteristics as the code 92 epoxy resin used in the prepregs. Thus, it is implicitly assumed that the manufacturing of the base-line laminate (face 1) and the reinforcement (face 2) has been cured simultaneously. The properties of the bulk epoxy resin are:

Elastic properties: E_a= 2350.0 MPa, ν_a=0.4.

Adhesive layer thickness: t_a=0.01 mm (this value can only be estimated, as it will be very difficult in practice to measure the thickness of the resin rich interface layer between the plies).

The CFRP-sandwich thickness drop-off zone configuration is illustrated "to scale" in Fig. 5, from which it is seen that the honeycomb cell-size s is rather large compared to the thicknesses of the CFRP-laminates. The question about whether the elastic foundation approach can be justified under such circumstances will be discussed in later section of this report.

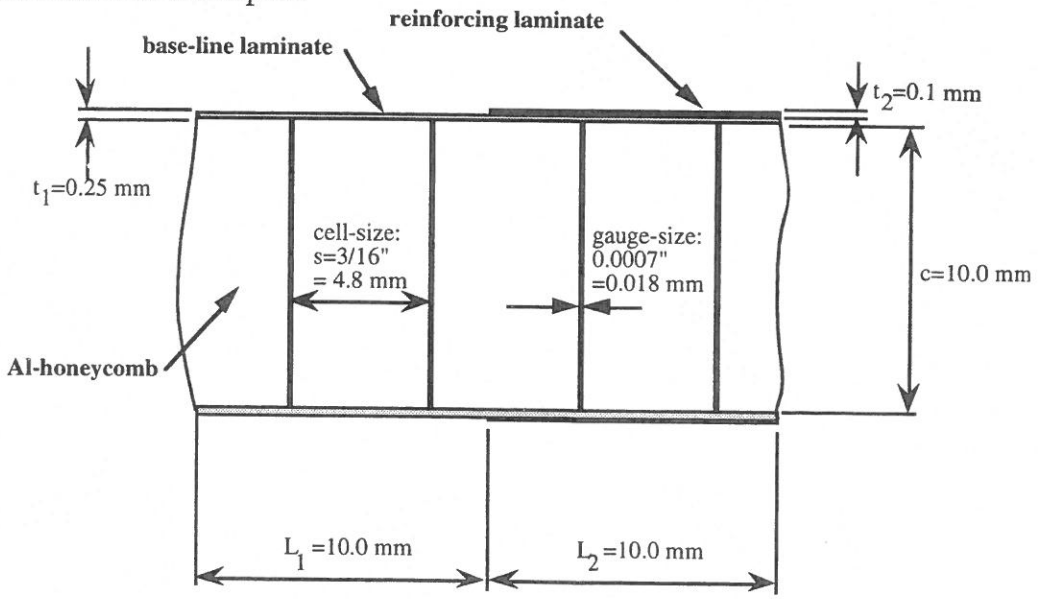

Fig. 5. "To scale" illustration of the considered CFRP-sandwich thickness drop-off problem.

In the example, the load is assumed to a unit compressive load applied at x=0, i.e., N_1=-1.0 N/mm (or P=1.0 N/mm). The main results of the analysis are shown in Figs. 6-11.

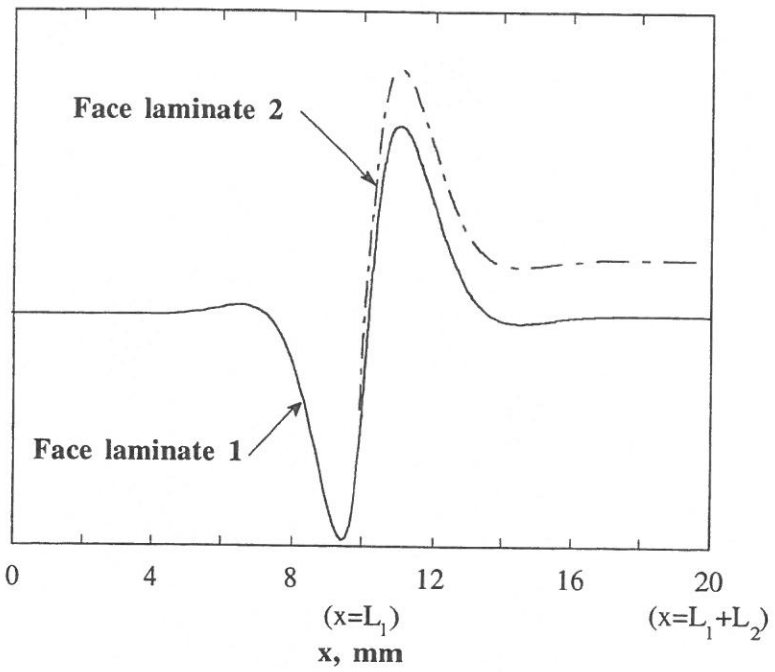

Fig. 6. "Scaled" plot of face laminates 1 and 2 in deformed configuration (solid and "dash-dot" lines represents the middle surfaces of the face laminates).

Fig. 6 shows the deformed configuration, where the magnitude of the deflections has been represented in scaled "non-dimensional" form. The reason for this is, that the magnitude of the maximum lateral deflections ($(w_1)_{max} \approx -1.5\ 10^{-5}$ mm at $x \approx 9.5$ mm) is several orders of magnitude smaller than the distance between the neutral-axes of the two face-laminates, thus making it impossible to show the deflections (in dimensional form) of the two face-laminates in the same graph.
It is observed from Fig. 6 that very strong local bending effects are present close to the thickness "drop-off", and that these effects diminishes very dramatically as the distance from the thickness "drop-off" is increased. The very distinct "wavy" harmonic nature of the deflectional pattern is caused by the core/face-interaction, and the wave-length of the elastic deformations can be calculated from the following expressions (refs. 1 and 2):

$$(14) \qquad \lambda = 2\pi L_0, \quad L_0 = \sqrt[4]{\frac{D_1^*}{K_z}}$$

where L_0 is referred to as the characteristic length of the core/face-interaction (or rather the foundation/face-interaction), and D_1^* the bending stiffness of the face-laminates. In region 1, D_1^* is equal to D_1 of face-laminate 1, whereas in region 2, D_1^* is equal to the combined bending stiffness of face laminates 1 and 2. Thus, eq. (14) predicts that λ should be of different magnitude in regions 1 and 2. This result is confirmed from a closer inspection of Fig. 6. Using eq. (14), λ(region 1)$\approx$4.0 mm and λ(region 2)$\approx$4.9 mm.

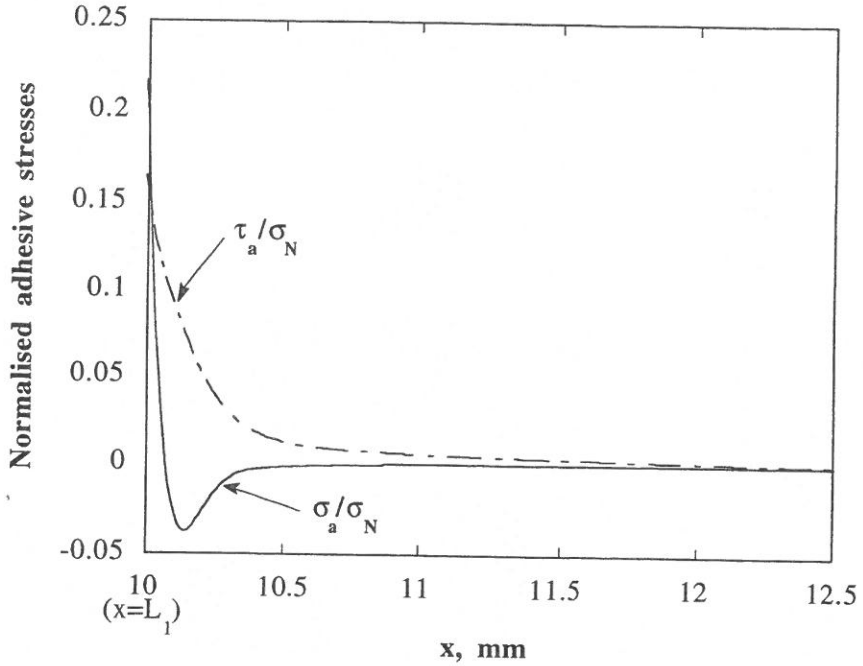

Fig. 7. Distribution of normalised adhesive/resin stresses: σ_a / σ_N, τ_a / σ_N.

Fig. 7 shows the distribution of peel and shear stresses in the adhesive layer. The adhesive stresses have been normalised with respect to the nominal stress defined by:

$$(15) \qquad \sigma_N = \frac{N_1(x=0)}{t_1} = \frac{-P}{t_1} = -4.0\,MPa$$

As expected, the presence of the adhesive peel and shear stress components is a very local phenomenon. Thus, it is seen that the decay of the adhesive stresses is nearly complete for x>12 mm. The peak values of σ_a/σ_N, τ_a/σ_N are located at $x=L_1$ (x=10.0 mm), i.e., at the free surface of the adhesive layer. The occurrence of non-zero shear stresses at the free edge of course violates the condition of stress equilibrium at this location, and is a consequence of modelling the adhesive layer as continuous compression/tension- and shear-springs rather than an elastic continuum. However, the true shear stress peak-value is located only a few adhesive thicknesses inward from the free surface, and the predicted peak value correlates well with the results of more advanced theoretical models.

Fig. 8 shows the distribution of normalised foundation stresses (interface) over the length L_1+L_2. As the honeycomb core material really does not supply a continuous support, but rather a discrete support, for the face laminates, the actual stresses (σ_c/σ_N, τ_c/σ_N) shown in Fig. 8, should be considered as an average stress distribution. However, the tendencies observed from the figure are clear. The interface transverse normal stresses follows a pattern similar to the transverse deflections of the face laminates. This is no surprise, of course, as the face/foundation interaction equations

(3) assumes the interface transverse normal stress component σ_c to be proportional with the lateral displacement w_1 of face-laminate 1.

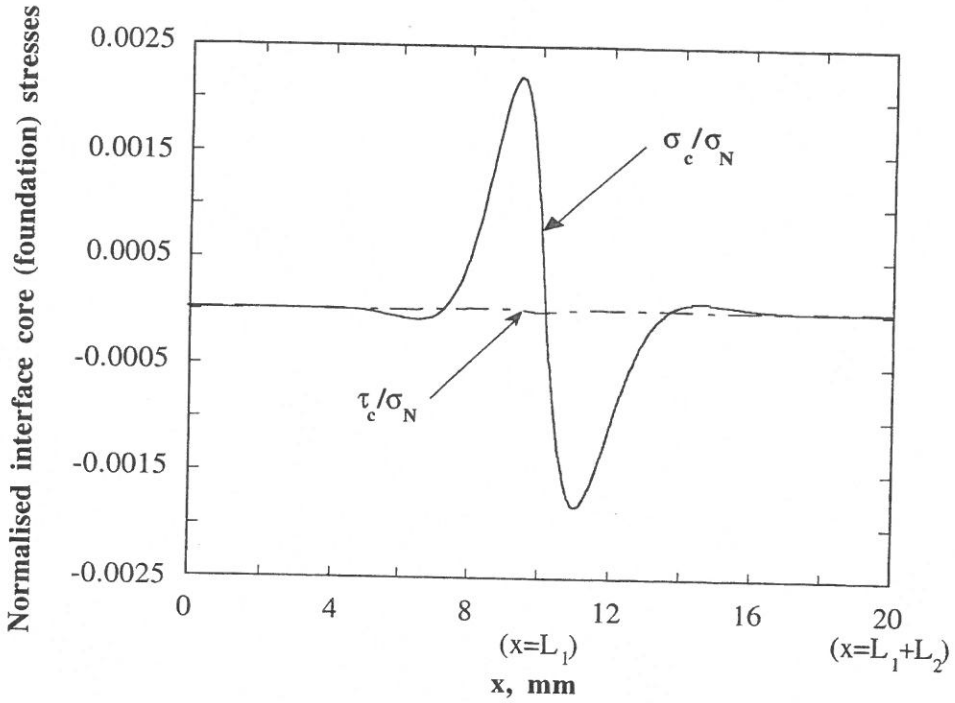

Fig. 8. Distribution of normalised foundation stresses: σ_c/σ_N, τ_c/σ_N.

Thus, it is seen that the presence of interface transverse normal stresses is also a very local phenomenon. Two peak values of σ_c/σ_N are observed, one compressive peak for $x<L_1$, and one tensile peak for $x>L_1$ (of course reversed if the external load is changed to a tensile load). The peak values are located approximately one quarter of an elastic wavelength ($\lambda/4$, se eq. (14)) away from $x=L_1$. In the actual case, the maximum interface transverse normal stress is compressive and is located in region 1 ($x<L_1$): $(\sigma_c/\sigma_N)_{peak}\approx 0.0025$. The corresponding peak value of σ_c/σ_N in region 2 is tensile: $(\sigma_c/\sigma_N)\approx -0.0018$. These peak values are quite modest in magnitude compared to the stresses in the adhesive layer, but it has to be remembered that the honeycomb-core material is a low density material with very limited crushing strength (Al honeycomb, 3/16"-5056-0.0007": $\sigma_{crushing}\approx 0.5$ MPa).

The distribution of normalised interface shear stresses (τ_c/σ_N) is also shown in Fig. 8, but as their magnitude are insignificant compared to σ_c/σ_N it can be concluded that the shearing interaction between core and face-laminates are of very little importance in the present problem.

The distributions of normal stress (N_1, N_2), bending moment (M_1, M_2) and transverse shear stress resultants (Q_1, Q_2) are shown in Figs. 9, 10, 11.

From Fig. 9 it is seen that the normal stress resultant in face-laminate 1 is constant in region 1 ($x<L_1$): $N_1/N_1(x=0)=1$. At the location of the thickness drop-off, a part of the normal stress loading is transferred into the reinforcing laminate (face-laminate 2) where the load-transfer is achieved through the shearing of the adhesive layer. The

normal stress resultant distribution in region 2 ($x>L_1$) stabilises rapidly to a constant value distribution, where face-laminate 2 carries approximately 14% of the total in-plane loading.

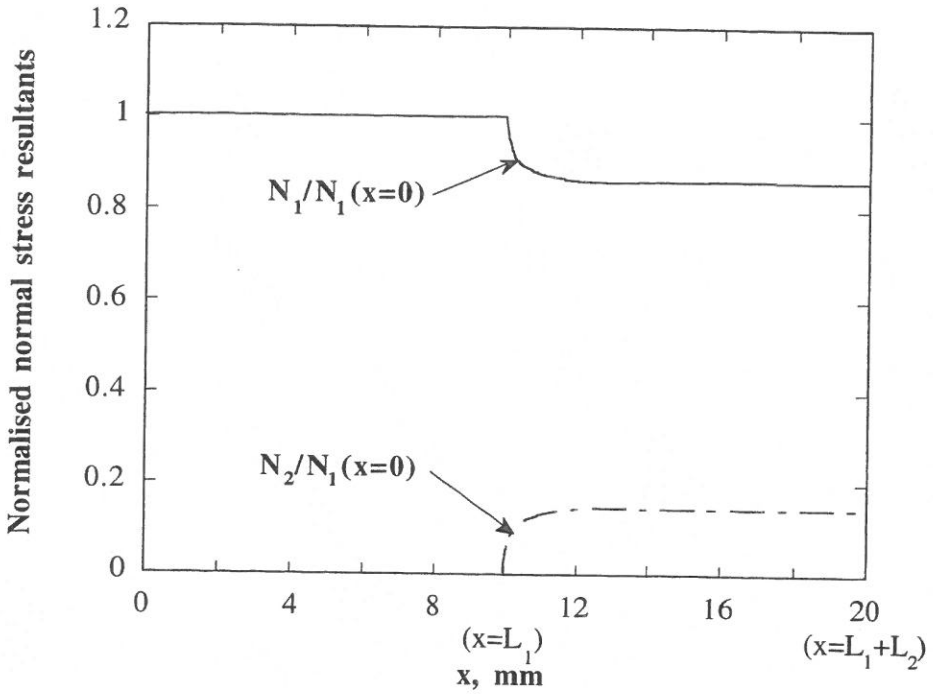

Fig. 9. Distribution of normalised normal stress resultants: $N_1/N_1(x=0)$, $N_2/N_1(x=0)$.

Fig. 10 displays the bending moment resultant distributions in the two face-laminates. As could be expected, significant bending moment concentrations are present (primarily in face-laminate 1) in the close neighbourhood of $x=L_1$, which of course is induced by the abrupt change of bending stiffness at this location.
The presence of these local bending moment concentrations, off course, also indicates the presence of severe stress concentrations in the face-laminates. The normal stress distributions within each of the laminae of the two face-laminates can be evaluated from the following expression:

$$(16) \qquad \sigma_{i,j} = \frac{N_i}{(A_{11})_i}\left[\frac{E_{11}}{(1-\nu_{12}\nu_{21})}\right]_{i,j} + \frac{M_i}{(D_{11})_i}\left[\frac{E_{11}}{(1-\nu_{12}\nu_{21})}\right]_{i,j} z_{i,j}$$

where i=1,2 refers to the actual face-laminate, and $j=1,..,n_i$ refers to the layers (or laminae) of which the face-laminates are composed.

Finally, Fig. 11 shows the distribution of transverse shear stress resultants within the two face-laminates. It is observed that the occurrence of transverse shear stress resultants is a very local phenomenon, and that their magnitude is quite small compared to the primary in-plane loading (N_1). However, the presence of local shear stress concentrations is yet another measure/indication of the presence of strong local bending effects in the neighbourhood of the thickness drop-off at $x=L_1$.

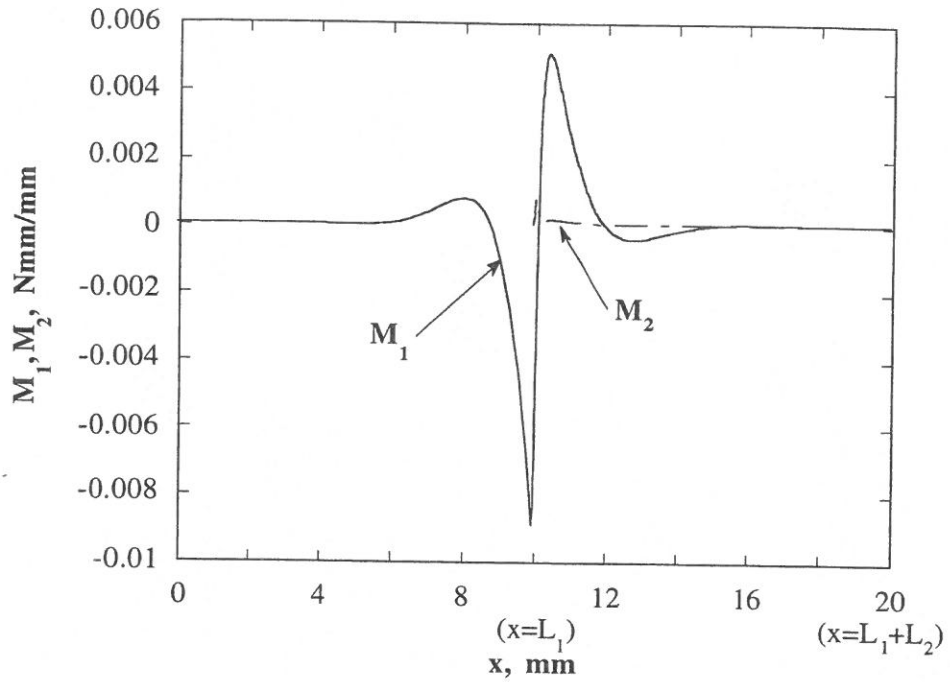

Fig. 10. Distribution of bending moment resultants: M_1, M_2 (unit load case: $N_1(x=0)$=-1.0 N/mm).

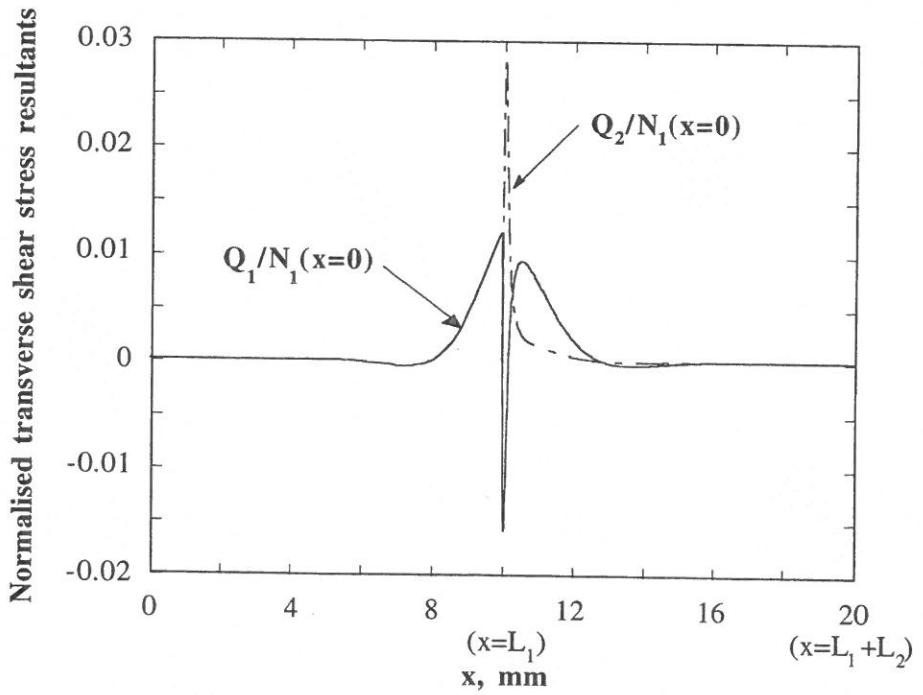

Fig. 11. Distribution of normalised transverse shear stress resultants: $Q_1/N_1(x=0)$, $Q_2/N_1(x=0)$.

To conclude this example, some important points should be emphasised. The presence of a thickness drop-offs exerts significant influence on the local stress distribution, an this could lead to a premature failure due to:

- inducement of stress concentrations in the interface between the core material and the face-laminates;
- inducement of stress concentrations in the adhesive/resin-layer interfacing the base-line face-laminate and the reinforcing laminate;
- and finally inducement of strong local bending stresses in the face-laminates.

6.2 Example 2: "unsupported thickness drop-off"

The example presented in this section is identical to example 1, except that the face-laminates are not supported by a core-material. Thus, the problem addressed is the classical bonded "doubler"-problem. This problem can be modelled simply by assigning zero-value elastic modulus to the core (i.e., E_c=0) in the input-data for the MATLAB® solution-procedure.
The reason for giving this example together with the first one, is to show that the presence of a supporting core material exerts a significant influence on the deflectional and load-distribution characteristics of the problem. Thus, it will be demonstrated that the inclusion of the core/face-laminate interaction in the modelling, is very important for the proper understanding of the mechanics of the local bending problem associated with face-laminate thickness drop-offs in CFRP-sandwich panels.

The geometrical, material and load data (compressive unit load) are as quoted for example 1. The results of the analysis of the bonded "doubler-problem" are shown in Figs. 12-16.

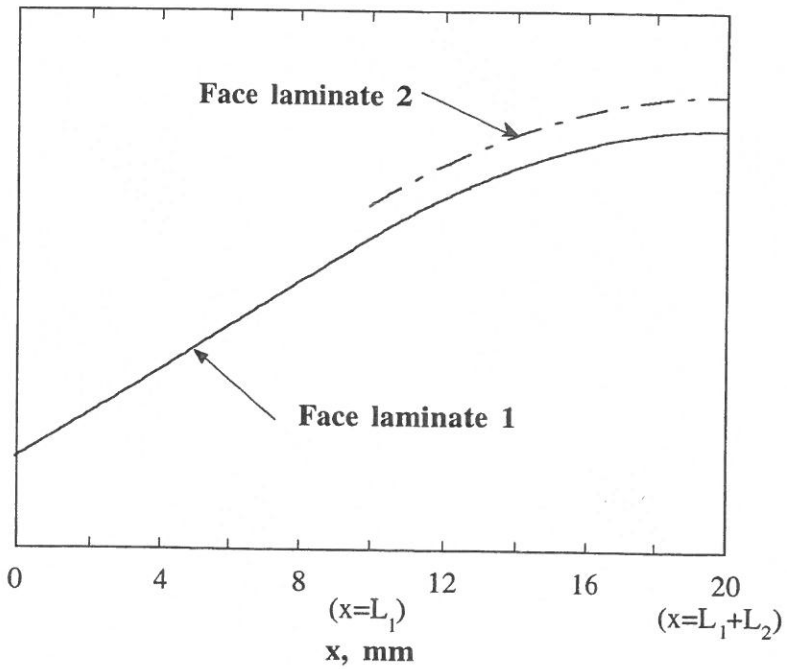

Fig. 12. Deformed configuration of face-laminates 1 and 2 for the bonded "doubler"-problem.

Fig. 12 shows the deformed configuration of the bonded "doubler", where the magnitude of the lateral deflections has been greatly exaggerated. Comparing Fig. 12 with Fig. 6 (supported face-laminates) illustrates that the principal elastic response is completely different for the two examples. Thus, it is observed, that the wavy harmonic "short wave-length" response which was seen in example 1 is completely missing in the solution to the bonded "doubler" problem.
Another important feature of the bonded "doubler" solution, as compared to example 1, does not show in Figs. 6 and 12 because the lateral deflections are only displayed qualitatively. As mentioned in the discussion of the results displayed in Fig. 6, the peak lateral deflection determined for example 1 was $(w_1)_{max} \approx -1.5\ 10^{-5}$ mm at $x \approx 9.5$ mm (very close to $x=L_1$), whereas the maximum lateral deflection determined in example 2 (same load !) was $(w_1)_{max} \approx 1.8\ 10^{-2}$ mm at $x=L_1+L_2=20$ mm. In other words, the supporting core material in example 1 acts as an effective restraint on the lateral deflections (to a degree of three orders of magnitude), with the very important side effect of inducing the characteristic wavy deflectional pattern displayed in Fig. 6.

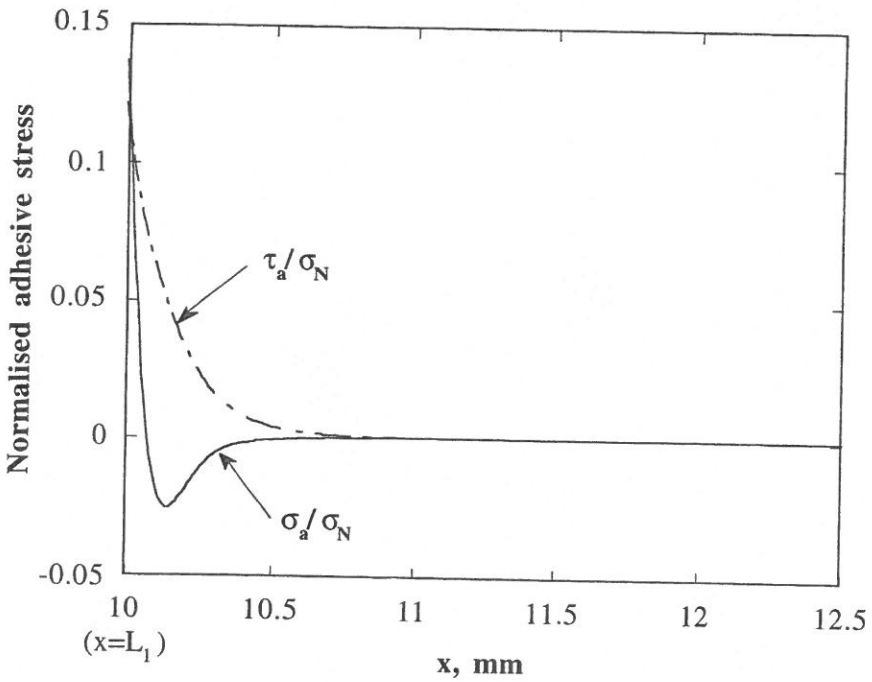

Fig. 13. Distribution of normalised adhesive/resin stresses: $\sigma_a / \sigma_N, \tau_a / \sigma_N$

The stress distribution within the adhesive/resin layer interfacing the two laminates is shown in Fig. 13. Comparing Figs. 13 and 7 displays the same overall tendency of very localised occurrence of adhesive stresses, but also reveals the somewhat surprising result that the peak interface adhesive/resin stresses obtained in example 2 have been reduced by approximately 40% as compared to example 1. The reason for this difference is, that the short wave-length elastic response imposed on the face-laminates in example 1 causes the difference between the displacements (in-plane as well as lateral) of the base-line and reinforcing laminates to exceed those encountered in example 2, thus inducing more severe local adhesive/resin stress concentrations (as the adhesive/resin stresses are proportional to the difference between the displacements of the two laminates according to eqs. (7)).

This observation reveals that the adhesive/resin layer stress concentrations in tapered CFRP face-laminates of sandwich panels, in general exceeds those experienced in unsupported CFRP-laminates. This again implies, that the *employment of the well-known bonded doubler results*, for the estimation of local stress concentrations in tapered CFRP-faced sandwich panels, will *seriously underestimate the adhesive/resin stress concentrations* in many cases.

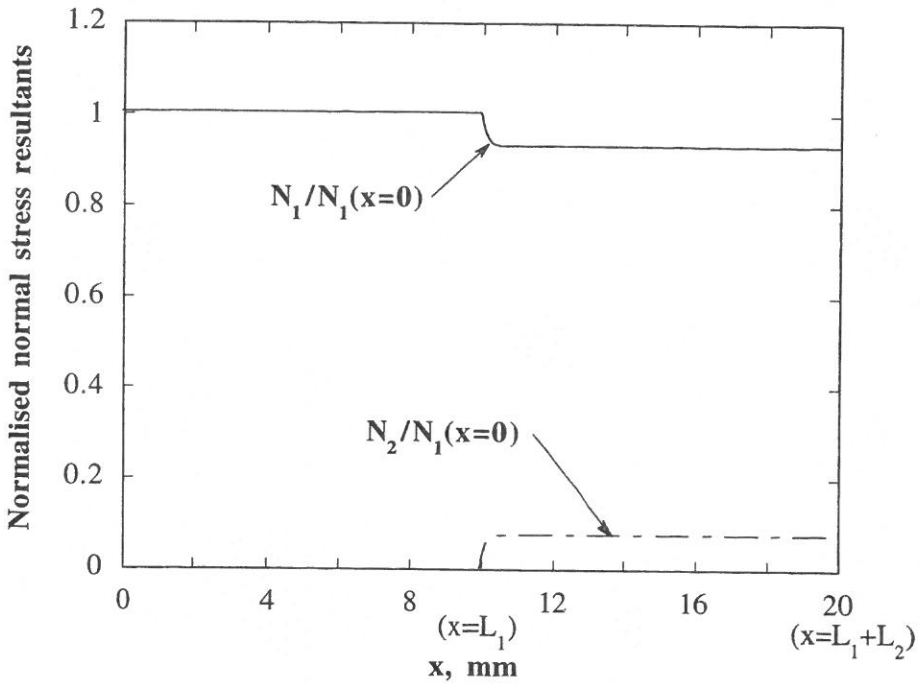

Fig. 14. Distribution of normalised normal stress resultants: $N_1/N_1(x=0)$, $N_2/N_1(x=0)$.

Considering the distribution of normal stress resultants in the two laminates, displayed in Fig. 14, it is seen that no major differences are present. The only slight deviation between the two examples (see Fig. 9 for comparison), is that the reinforcing laminate carries an even smaller portion (about 8%) of the overall in-plane load than was the case in the first example.
The explanation for this phenomenon can be given simply by considering the fourth of the equilibrium equations (6), i.e. $N_2'=\tau_a$. This equation states, that the rate of change of the normal stress resultant N_2 in face-laminate 2 equals the adhesive/resin layer stress τ_a. As τ_a is of considerable lower magnitude, as well as extends with non-zero values over a considerably shorter distance, in the present example as compared to example 1, it is apparent that the build up of the normal stress resultant N_2 in the reinforcing laminate is less significant than in example 1. This again indicates, that the reinforcing laminate in *unsupported CFRP-laminates generally participates less in the carrying of in-plane loads than is the case for CFRP-faces of sandwich panels.*

The bending moment resultant distribution is displayed in Fig. 15, and comparison with Fig. 10 shows a significantly different overall pattern. This pattern, of course, is closely associated with the deflectional pattern shown in Fig. 12. From Fig. 15 it is

seen that no bending effects ($M_1 \approx 0$) are present in face-laminate 1 for $x<L_1$, while an almost constant value of M_1 is present for $x>L_1$ ($M_1 \approx 0.013$ Nmm/mm). These observations corresponds very well with Fig. 12, where the "straight-line"/"zero curvature" deflectional pattern seen for $x<L_1$ indicates that no bending moment loading is being transferred in this area. For $x>L_1$, Fig. 12 displays a "constant curvature"/"circular arc" deflection pattern, thus indicating the transfer of a constant bending moment loading.

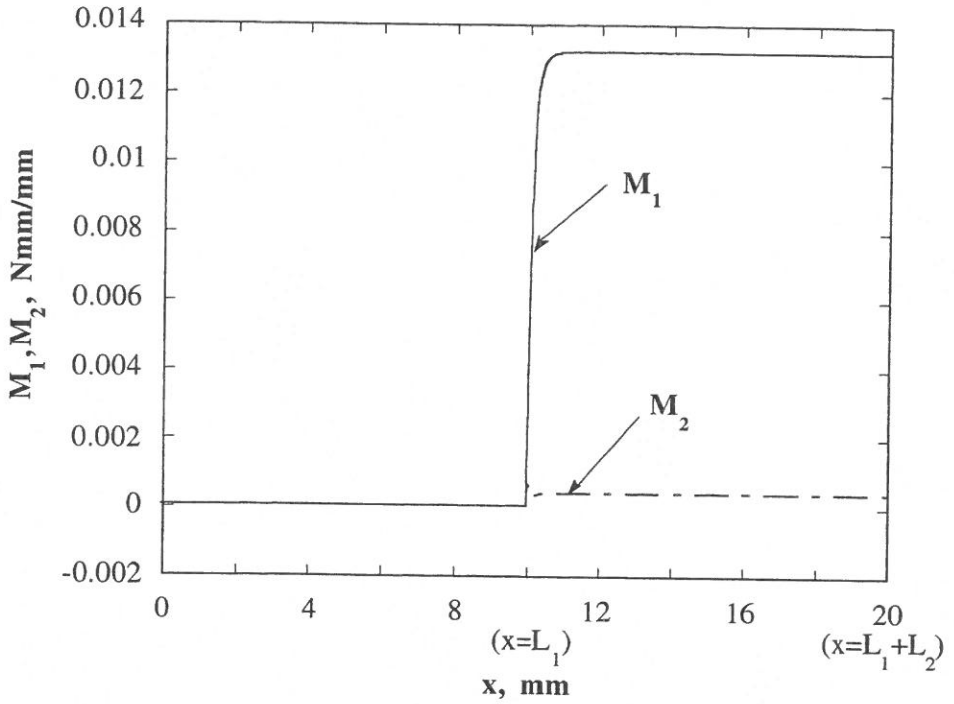

Fig. 15. Distribution of bending moment resultants: M_1, M_2 (unit load case: $N_1(x=0)=-1.0$ N/mm).

Face-laminate 2 does not contribute significantly to the bending moment load transfer.
Comparing with the results displayed in Fig. 10, it is also observed that the magnitude of the peak value encountered (present example: $(M_1)_{peak} \approx 0.013$ Nmm/mm) is somewhat larger than was experienced in the former example (example 1: $(M_1)_{peak} \approx -0.009$ Nmm/mm). This result, which holds generally true, shows that the bending stresses encountered for the unsupported doubler case exceeds the locally induced bending stresses encountered in sandwich panels.

Finally, Fig. 16 displays the transverse shear stress resultant distribution for the unsupported thickness drop-off problem. As expected, transverse shearing effects are only present very close to $x=L_1$. Thus, a complete decay of Q_1 and Q_2 is observed within 0.5 to 1 mm from $x=L_1$. These observations are in close agreement with the results shown in Fig. 15, as the constant moment regions invariably (follows from the elementary theory for bending of beams) corresponds to regions of zero transverse shearing.

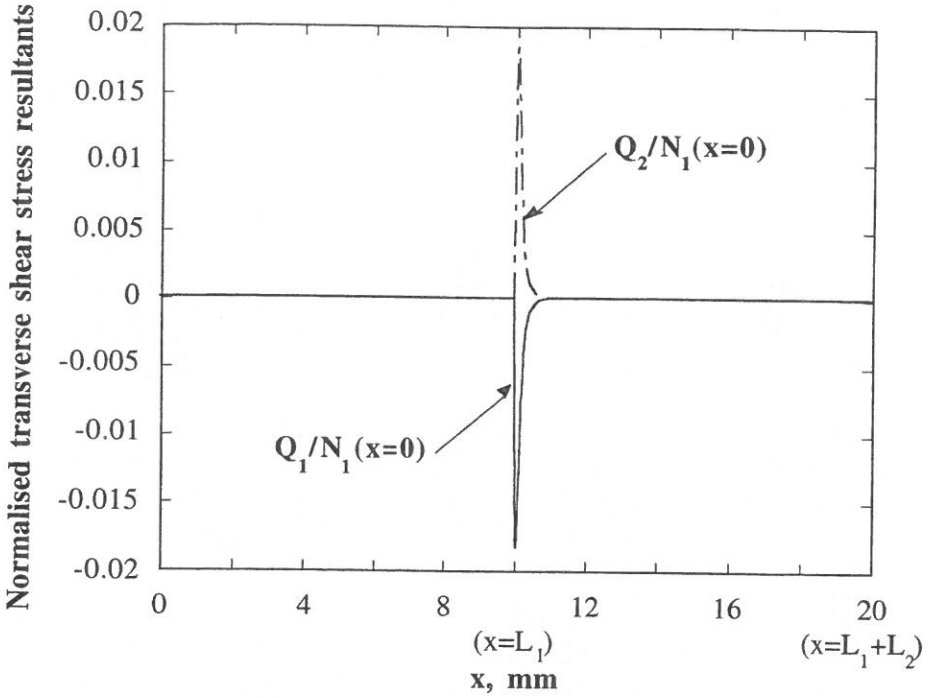

Fig. 16. Distribution of normalised transverse shear stress resultants: $Q_1/N_1(x=0)$, $Q_2/N_1(x=0)$.

7. *LIMITATIONS AND RANGE OF APPLICABILITY*

To conclude the presentation of the mechanical model introduced in the present study, a few additional comments about the implications and limitations of the model will be given.

The method presented in the preceding chapter relies heavily upon the assumption that the face-laminate/core interaction can be modelled properly by use of an elastic foundation model (two-parameter foundation model in the present case). Obviously, the application of such a model cannot be justified in a general sense as it is impossible to specify constant values of the elastic foundation moduli K_z, K_x which are appropriate for deformations of any (arbitrary) deflectional wave-length λ (defined by eqn. (14)). The reason for this is that the shearing deformations of the core material (foundation) becomes very influential for deformations with very short wave-length, thus implying that proper modelling of the face-laminate/core interaction can only be achieved by application of a continuum formulation for the core-material. For practical sandwich panels, however, the bounds imposed by the vaguely formulated concept of "deformations with very short wave-length" are not likely to be active, as the values of the bending stiffness D_1 and the foundation modulus K_z observed even for extremely thin CFRP-laminates (2-3 plies) in combination with high-density/high-stiffness Al-honeycomb cores, as seen in special spacecraft applications, will ascertain sufficiently large deflection wave-lengths to ensure that the elastic foundation approach will supply good results. As a "rule of thumb", the elastic foundation approach will generally provide good result if the following inequality is satisfied (t_1 is the thickness of the base-line face-laminate):

(17) $\lambda >> t_1$

Another important point to be made, in the context of evaluating the quality of the suggested approach, is that the modelling of the core by application of an elastic foundation model implies that the core material is assumed to support the face-laminates continuously. This, off course, is not strictly true for honeycomb-cored sandwich panels where the face-laminates are supported in a discrete manner along the edges of the individual honeycomb-cells. Whether the elastic foundation approach provides a good mechanical model for the face/core-interaction is determined by two important quantities: the wave-length of the elastic deformations λ, and the cell-size of the honey-comb which is denoted by "s". The following guidelines can be given:

(18)

$\lambda \geq s$: The elastic foundation model provides a **good** description, and the quality of the model improves dramatically if $\lambda >> s$.

$\lambda < s$: The elastic foundation model is **not adequate**, as the face-laminates will tend to act as plates within the boundaries of each honeycomb-cell. The quality of the elastic foundation model of course degrades drastically if $\lambda << s$.

For the main portion of honeycomb-cored CFRP-sandwich panels (even for space-applications) the elastic foundation approach will provide a good description as the former of the inequalities (18) will be fulfilled. However, for certain space-applications, CFRP-sandwich panels with extremely thin CFRP face-laminates in combination with low stiffness honeycombs (light gauge, large cell-size) are used, and for such cases the elastic wave-lengths encountered can be very close to (or even violate) the limits imposed by the inequalities (18).
For instance, this was the case in example 1 (section 6.1) where the elastic wave-length of face-laminate 1 was found to be $\lambda \approx 4.1$ mm, whereas as the honeycomb cell-size was assumed to be s=3/16"≈4.8 mm (see Fig. 5 for scale-sizes of problem). Thus, it is seen that the application of the elastic foundation approach for the analysis of example 1, at its very best, has to be considered as a limiting case, and that the actual numerical results obtained have to be looked upon with some reservation.

8. PARAMETRIC EFFECTS

The two examples given in chapter 6 displayed most of the basic mechanical features for the general thickness drop-off problem (supported as well as unsupported). However, to obtain an understanding for the influence of the various parameters included in the modelling of the problem, it is necessary to conduct a parametric study.

The parametric effects included in the present study are:

- the bending stiffnesses of face-laminates 1 and 2.
- the core transverse stiffness.
- the stiffness of the adhesive/resin interface layer between face-laminates 1 and 2.

The influence of these quantities on the local bending behaviour will be illustrated by showing the peak values of the adhesive stresses components σ_a, τ_a, the core transverse normal stress σ_c (due to its almost negligible magnitude τ_c will not be shown, see Fig. 8), and finally the laminate bending moment resultants M_1, M_2 as functions of the following three parameters:

- the characteristic length of face-laminate 1: $L_0 = \sqrt[4]{\frac{D_1}{K_z}}$.
- the ratio of the bending stiffness of face-laminate 2 (reinforcement) to the bending stiffness of face-laminate 1 (base-line laminate): $\frac{D_2}{D_1}$.
- and finally the ratio of the adhesive/resin layer stiffness (E_a/t_a) to the transverse foundation modulus K_z (core stiffness): $\Lambda = \frac{(E_a / t_a)}{K_z}$.

Note that L_0 has the dimension mm (length), whereas D_2/D_1 and Λ are non-dimensional parameters.
The external load is assumed to be a unit **compressive** normal stress resultant imposed on the structure at x=0. Thus the external load is given as $N_1(x=0)=-P=-1.0$ N/mm. In the parametric study, the face-laminate bending and extensional stiffnesses D_1, D_2, A_1, and A_2 are treated as variables, whereas (for reasons of simplicity) the thicknesses of the face-laminates are assumed to be identical and constants: $t_1=t_2=0.5$ mm (the face-thicknesses are parameters of "secondary" influence as will be explained later in section 8.3). The core thickness c and the core E-modulus E_c are also assumed to be constants, which again implies that the foundation moduli are assumed to be constants in the parametric study (again for reasons of simplicity).
In the representation of the results obtained the adhesive and core stress components will be normalised with respect to the nominal stress defined by (similar to eq. (15)):

$$(19) \qquad \sigma_N = \frac{N_1(x=0)}{t_1} = \frac{-1.0 \text{ N/mm}}{0.5 \text{ mm}} = -2.0 \text{ MPa}$$

8.1 Stress and moment concentrations vs. L_0 and D_2/D_1 (fixed Λ)

For all the parametric effects given in this section the parameter Λ (representing the ratio of the effective adhesive stiffness to the core stiffness) is fixed to Λ=250.

The first parametric results, which are shown in Fig. 17, represents the normalised peak adhesive transverse normal stress σ_a/σ_N as function of L_0 and D_2/D_1. The peak value of σ_a/σ_N is located at $x=L_1$ (see Fig. 7). It should be noted from Fig. 17 that σ_a/σ_N is positive, and as σ_N is negative (compressive), it is seen that the stress state within the adhesive/resin layer is also compressive. For a tensile external load the adhesive transverse normal stresses would of course also be tensile.
The tendency observed from Fig. 17 is that σ_a/σ_N decreases significantly as L_0 is increased (i.e., as the bending stiffness of face-laminate 1 is increased compared to the core stiffness), and that σ_a/σ_N increases as D_2/D_1 is increased (i.e., as the bending stiffness discontinuity is increased). It is further observed that the stress range covered

(about 7 decades) is extremely large, thus indicating that a very strong "power law dependency" exists between σ_a/σ_N and L_0.
The range covered for the characteristic length L_0 is also very large; 0.25 mm $\leq L_0 \leq$ 100 mm (corresponding to elastic wave-lengths in the range 1.6 mm $\leq \lambda \leq$ 628 mm, according to eq. (14)). The range of L_0 which corresponds to "realistic" geometrical and material properties is not quite as wide as shown in Fig. 17 (and all the other figures to come), but would rather be 0.4-0.5 mm $\leq L_0 \leq$ 8-10 mm.

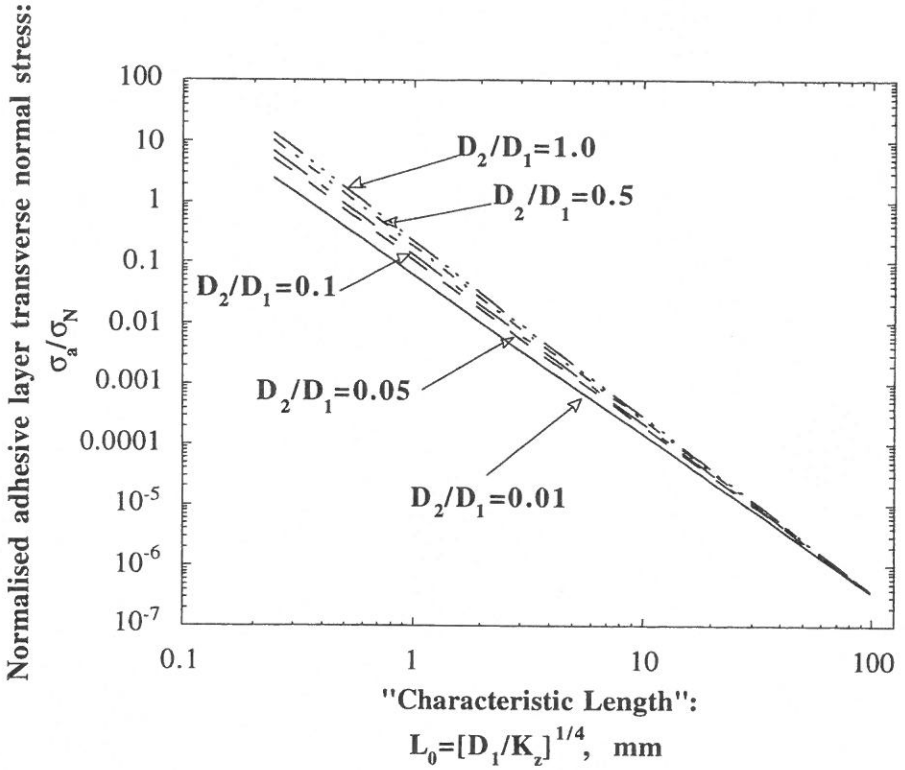

Fig. 17. Normalised peak adhesive transverse normal stress σ_a/σ_N vs. L_0 and D_2/D_1 (Λ=250).

At this stage an important point should be made. For the compressive load case considered, the peak adhesive transverse normal stress σ_a is compressive (as already mentioned), and this circumstance of course eliminates the possibility of delamination between face-laminates 1 and 2 to be a likely failure-mode in an actual engineering application. However, if the external load is tensile (due to overall tensile or overall bending loading of a sandwich panel) peeling would be a highly possible failure-mode.

Fig. 18 shows the normalised peak adhesive/resin layer shear stress τ_a/σ_N as function of L_0 and D_2/D_1. The peak value of τ_a/σ_N is located at $x=L_1$ (see Fig. 7).
The overall tendencies observed from Fig. 18 are similar to the ones observed from Fig. 17, i.e., the peak value of τ_a/σ_N decreases strongly as L_0 is increased, and increases (not so dramatically however) as D_2/D_1 is increased from D_2/D_1=0.01 to D_2/D_1=1.

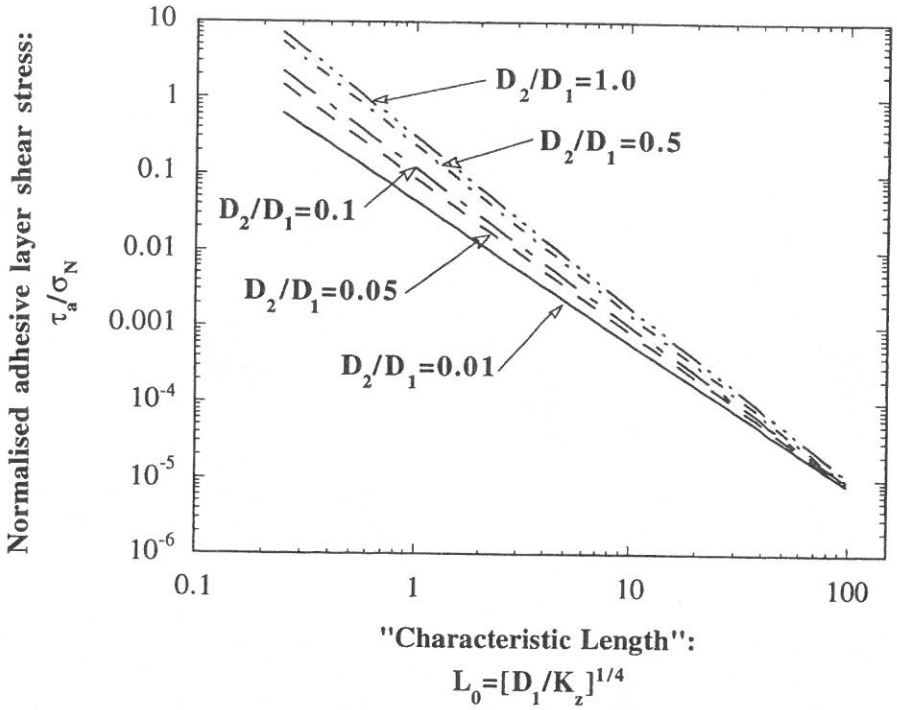

Fig. 18. Normalised peak adhesive shear stress τ_a/σ_N vs. L_0 and D_2/D_1 (Λ=250).

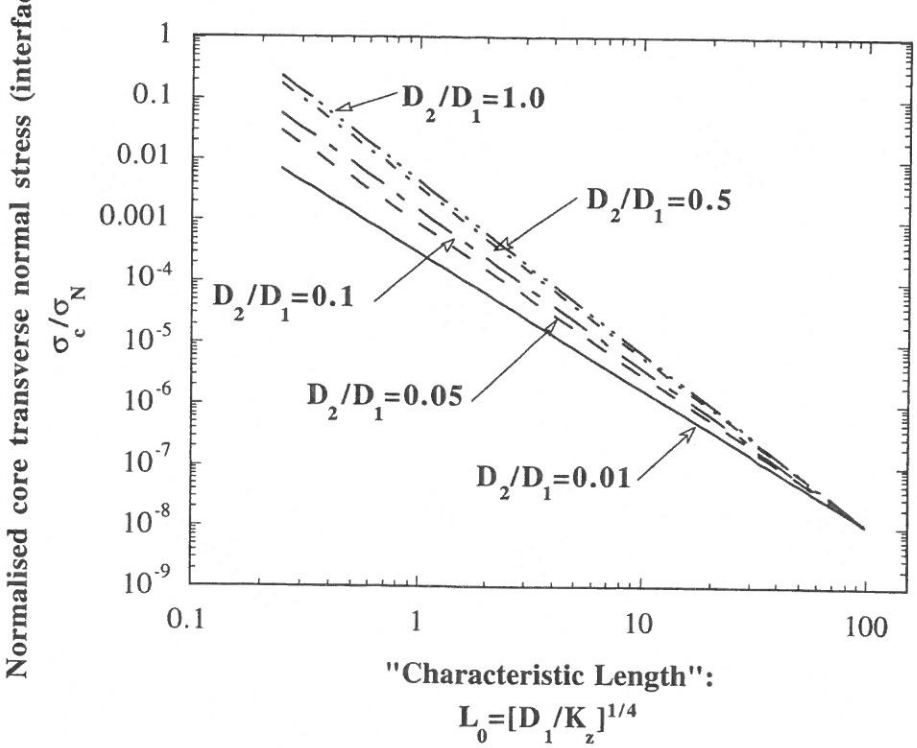

Fig. 19. Normalised peak core transverse normal stress σ_c/σ_N (interface between core and face-laminate 1) vs. L_0 and D_2/D_1 (Λ=250).

Fig. 19 shows the normalised peak core transverse normal stress σ_c/σ_N (interface between core material and face-laminate 1) as function of L_0 and D_2/D_1. As was the case for σ_a/σ_N (Fig. 17) it is noted that σ_c/σ_N is positive, and as σ_N is negative (compressive), it is observed that the peak core stress is compressive. The peak value of σ_c/σ_N is located approximately $\lambda/4 = 2\pi L_0/2$ before $x=L_1$, i.e. at $x \approx L_1-\pi L_0/2$ (see Fig. 8).
Again the overall tendencies observed from Fig. 19 are similar to the ones observed from Figs. 17 and 18, i.e., the peak value of σ_c/σ_N decreases strongly as L_0 is increased, and increases as D_2/D_1 is increased.

The last two figures (Figs. 20, 21) to be included in the this part of the parametric study illustrates the influence of the local bending on the stress state in the two face-laminates. Showing the actual peak bending stresses induced in the face-laminates would require an exact specification of the actual laminate lay-ups considered (including lay-up angles and stacking sequences for each of the face-laminates), and would therefore destroy the generality of the parametric results.
Instead, it has been decided to show the peak values of M_1, M_2 as function of L_0 and D_2/D_1. This provides for the desired generality of results, and for specified laminate lay-ups it is an easy task to evaluate the actual bending stress distributions (discontinuous) through the thickness of the laminates.
The inplane normal stress resultants N_1, N_2 in the two face-laminates will not be included in this parametric study as no real stress concentrations occurs (see Fig. 9). The peak values of transverse normal stress resultants Q_1, Q_2 will not be given either, even though significant peaks are induced (as illustrated in Fig. 11). However, the magnitudes of the transverse shear stresses, which over the laminate thicknesses adds up to the transverse shear stress resultants, are quite modest.

Fig. 20. shows the peak bending moment resultant M_1 induced in face-laminate 1 as function of L_0 and D_2/D_1. The peak value of M_1 is located approximately at the junction between regions 1 and 2, i.e. approximately at $x \approx L_1$.
It is observed that the peak value of M_1 is negative, thus indicating that the upper fibre of face-laminate 1 in a compressive state of stress at the location of $(M_1)_{peak}$. This latter observation is, of course, a direct consequence of the fact that face-laminate 1 is indented into the core material at the location where M_1 attains its peak value (see Figs. 6 and 10).
The overall tendency observed from Fig. 20 is that the peak value of M_1 (absolute value) decreases as the characteristic length L_0 increases, and increases as D_2/D_1 is increased. Thus, the general effects observed are similar to the parametric influences exerted on the peak adhesive and core stresses.
Even though the effect of altering L_0 and D_2/D_1 is very significant, the mere fact that a linear "Y-axis" is used to represent $(M_1)_{peak}$ in Fig. 20 reveals that the influence is not as strong as were the case for σ_a/σ_N, τ_a/σ_N , σ_c/σ_N (plots shown in Figs. 17, 18 and 19).

Fig. 21. shows the peak bending moment resultant M_2 induced in face-laminate 2 as function of L_0 and D_2/D_1. The peak value of M_2 is located approximately $\lambda/8 = \pi L_0/4$ after $x=L_1$, i.e. approximately at $x \approx L_1+\pi L_0/4$.

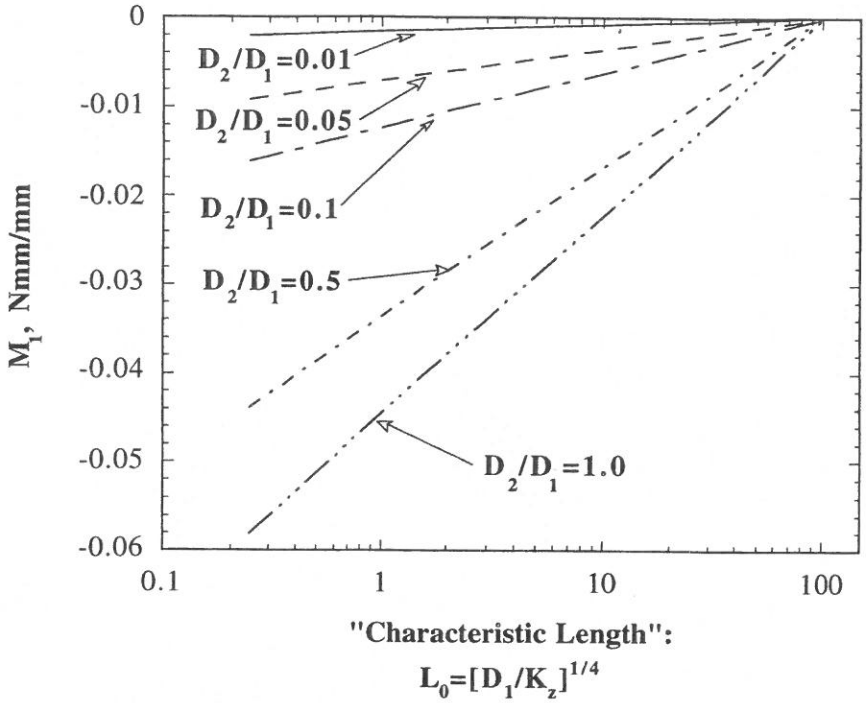

Fig. 20. Peak bending moment resultant M_1 in face-laminate 1 vs. L_0 and D_2/D_1 (Λ=250). External load: $N_1(x=0)$=-P=-1.0 N/mm (unit load).

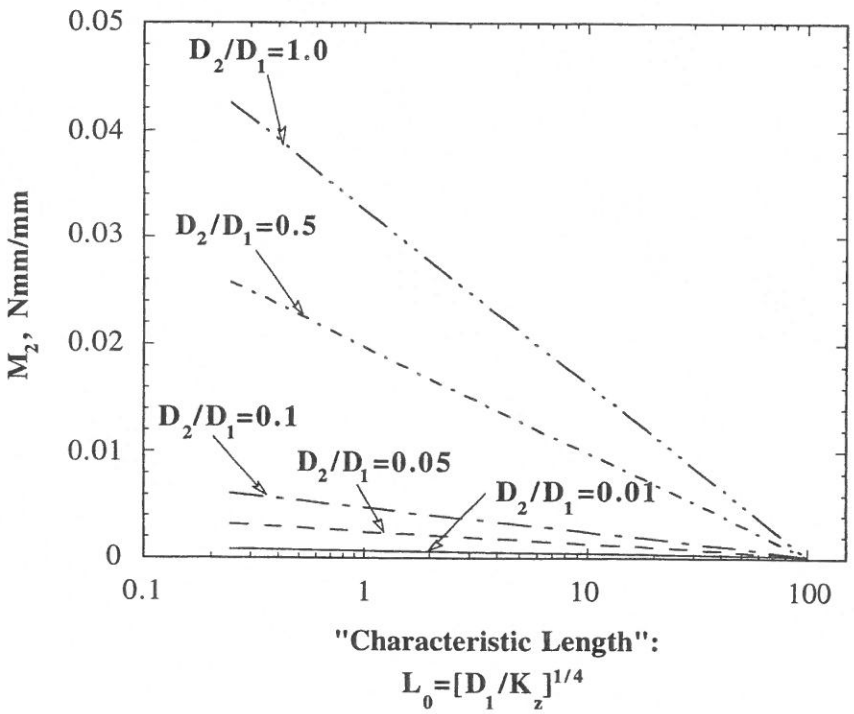

Fig. 21. Peak bending moment resultant M_2 in face-laminate 1 vs. L_0 and D_2/D_1 (Λ=250). External load: $N_1(x=0)$=-P=-1.0 N/mm (unit load).

The peak value of M_2 is positive, thus indicating that the upper fibre of face-laminate 2 is in a tensile state of stress at the location of $(M_2)_{peak}$.
Apart form this difference, and apart from the fact that the peak value of M_2 is generally smaller than the peak value of M_1, the overall pattern is the same as seen in Fig. 20. Thus, it is seen that $(M_2)_{peak}$ decreases with increasing L_0-values, and increases with increasing values of D_2/D_1.

Summing up briefly, the parametric study represented in this section has shown that the stress state in the constituent parts (core material, face-laminates and adhesive/resin interface layer), which together constitutes the thickness drop-off zone in a sandwich panel, is affected very strongly by L_0 and D_2/D_1. The general observation is, that the lower the value of L_0 (i.e., the shorter the wave-length of the elastic response) the more severe stress concentrations are encountered. Furthermore, it is observed that the magnitude of the stress concentrations increases with increasing vale of D_2/D_1 (i.e., with increasing values of D_2 for D_1=constant)

8.2 Stress and moment concentrations vs. L_0 and Λ (fixed D_2/D_1)

The parametric study presented in this section has been carried out by varying the characteristic length L_0 and the parameter $\Lambda=(E_a/t_a)/K_z$ which determines the ratio of the adhesive/resin layer stiffness to the core stiffness. The ratio between the bending stiffness of face-laminate 2 (reinforcement) to the bending stiffness of face-laminate 1 has been kept fixed to $D_2/D_1=0.05$ (which is a realistic value for the discontinuous jump in bending stiffness at a typical face-thickness drop-off in a CFRP-sandwich panel).

The first parametric effects given in this section are presented in Fig. 22, which shows the peak adhesive/resin normalised transverse normal stress σ_a/σ_N as function of L_0 and Λ.

The range of the parameter Λ is given as $50 \leq \Lambda \leq 2000$, which is a bit wide with respect to the upper end of the range. For "realistic" combinations of geometrical and material parameters Λ will usually be limited by $\Lambda < 1100\text{-}1200$.

The peak value of σ_a/σ_N is located at $x=L_1$, and as was the case for the results shown in Fig. 17 the fact that σ_a/σ_N is positive indicates that a compressive state of stress is present in the adhesive layer.

The general tendency derived from Fig. 22 is that σ_a/σ_N decreases with increasing value of L_0 (which was already shown in Fig. 17, section 8.1), and that σ_a/σ_N increases with increasing value of Λ. The latter of the observations made indicates that the adhesive layer stress state is very sensitive to the relative stiffness of the adhesive layer (E_a/t_a) to the stiffness of the core material (K_z), and that severe stress concentrations (up to 3-4) can be encountered in the "realistic" range of the characteristic length L_0: 0.4-0.5 mm $\leq L_0 \leq$ 8-10 mm.

Fig. 23 displays the normalised peak adhesive/resin shear stress τ_a/σ_N as function of L_0 and Λ. As could be expected the overall tendencies observed from Fig. 23 are similar to the tendencies observed from Fig. 22.

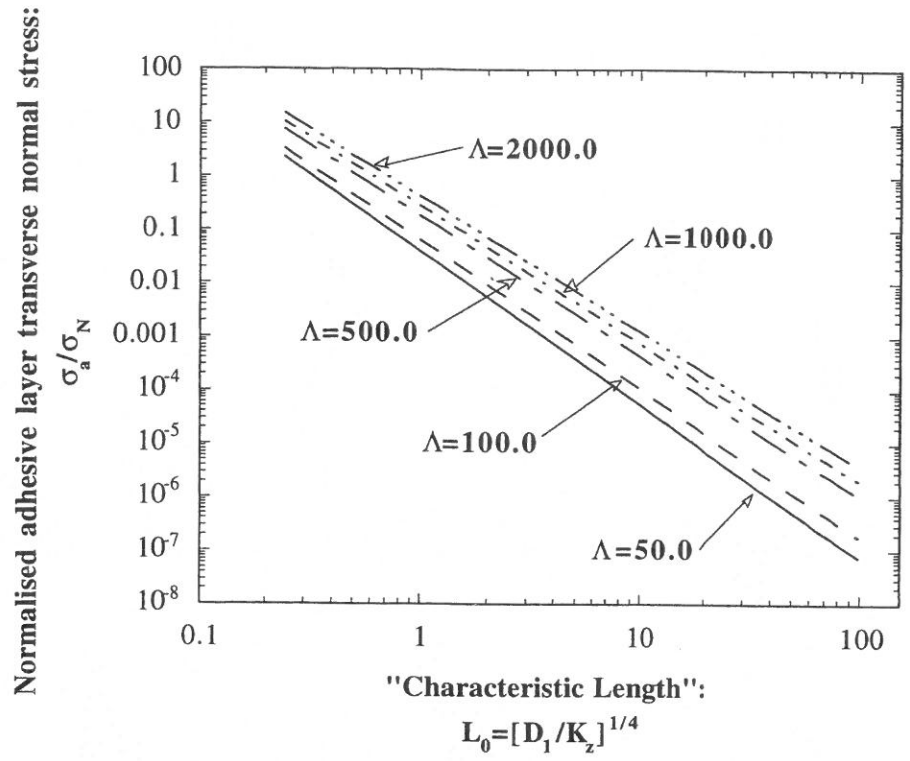

Fig. 22. Normalised peak adhesive transverse normal stress σ_a/σ_N vs. L_0 and Λ (D_2/D_1=0.05).

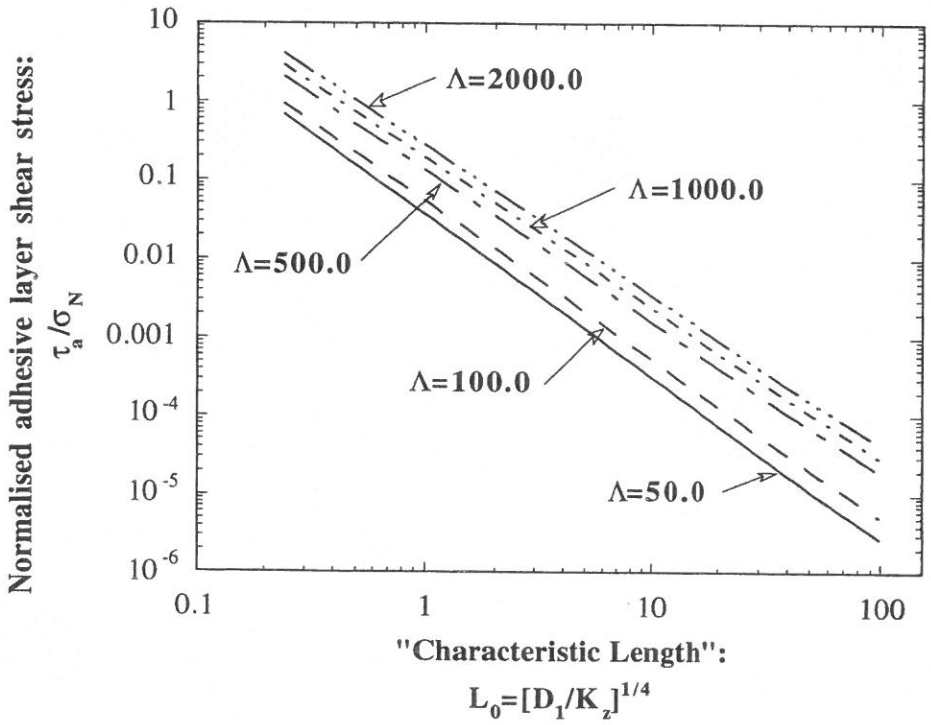

Fig. 23. Normalised peak adhesive shear stress τ_a/σ_N vs. L_0 and Λ (D_2/D_1=0.05).

Fig. 24 Shows the peak core transverse normal stress σ_c/σ_N (at the interface between core and face-laminate 1) as function of L_0 and Λ.
As expected from the results given in Fig. 19, the dependency of L_0 is pronounced, and the overall tendencies are exactly as stated in section 8.1. As was the case for the results presented in Fig. 19, the peak value of σ_c/σ_N occurs approximately at $x \approx L_1 - \pi L_0/2$. It should be noted that $(\sigma_c)_{peak}$ is compressive for the considered load case.
With respect to the relationship between the peak value of σ_c/σ_N and the parameter Λ, the tendency is that σ_c/σ_N increases with increasing Λ. Thus, it is observed that the core stresses increases as the stiffness of the adhesive/resin layer increases relative to the core stiffness. Even though the actual stress concentration values displayed in Fig. 24 might seem modest in magnitude, it should be remembered that the core material is usually a low density material with limited load carrying capability (compared with the face-laminates and the resin material).

The influence of L_0 and Λ on the peak value of the bending moment resultants M_1, M_2 in face-laminates 1 and 2, respectively, is displayed in Figs. 25 and 26. The overall tendencies with respect to the influence of the parameter L_0 are quite similar to the results displayed in Figs. 20 and 21 of section 8.1. Thus, it is seen that the peak values of M_1 (peak value negative), M_2 (peak value positive) decreases strongly as the characteristic length increases. This implies that the bending stress state in the face-laminates becomes less severe as the bending stiffness of the faces is increased relative to the core transverse stiffness.

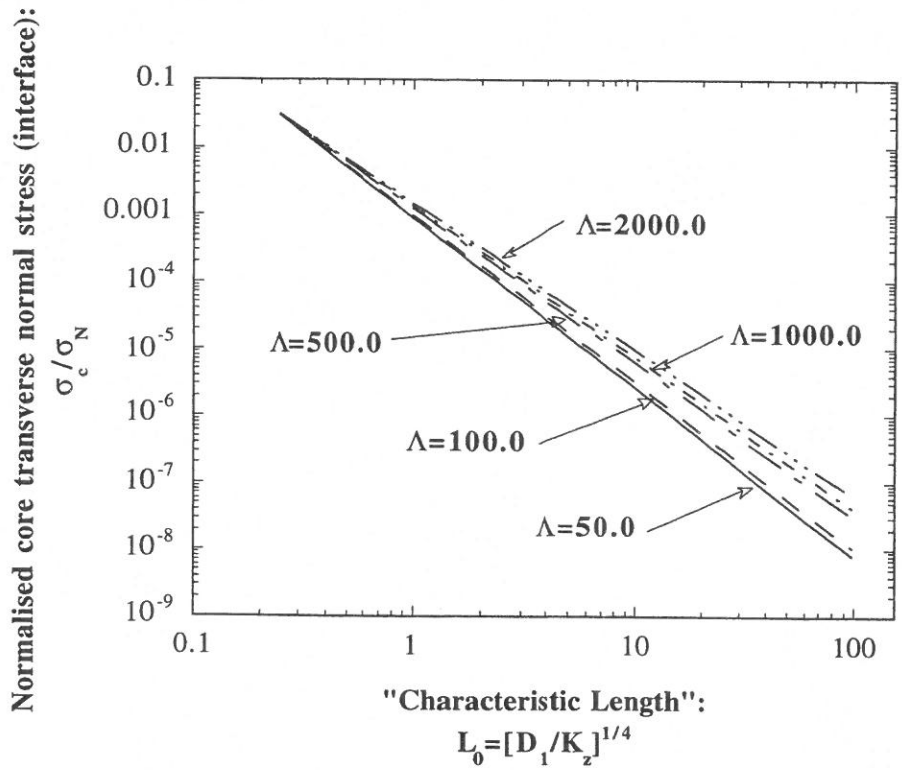

Fig. 24. Normalised peak core transverse normal stress σ_c/σ_N (interface between core and face-laminate 1) vs. L_0 and Λ (D_2/D_1=0.05).

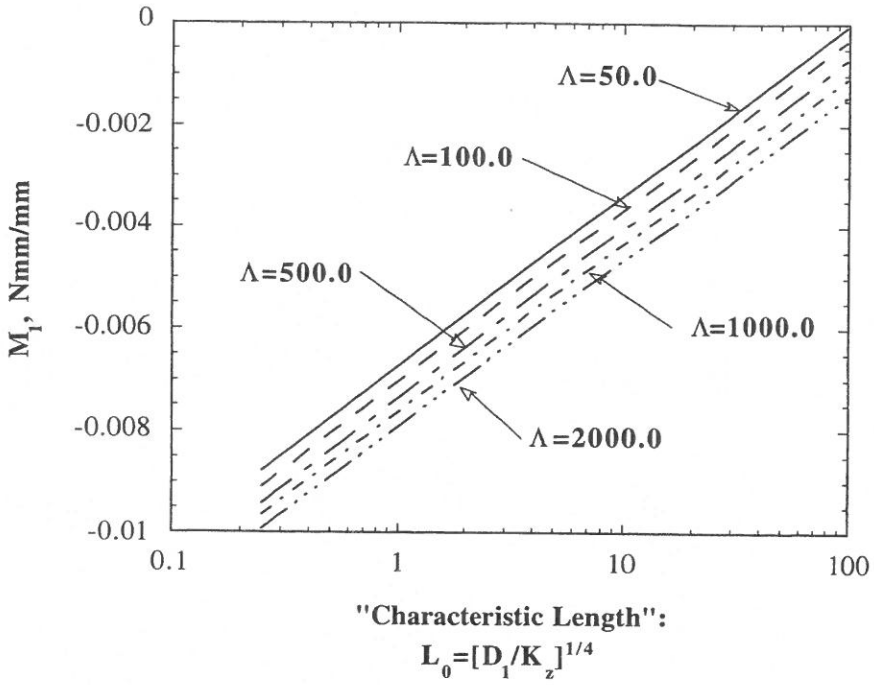

Fig. 25. Peak bending moment resultant M_1 in face-laminate 1 vs. L_0 and Λ (D_2/D_1=0.05). External load: $N_1(x=0)$=-P=-1.0 N/mm (unit load).

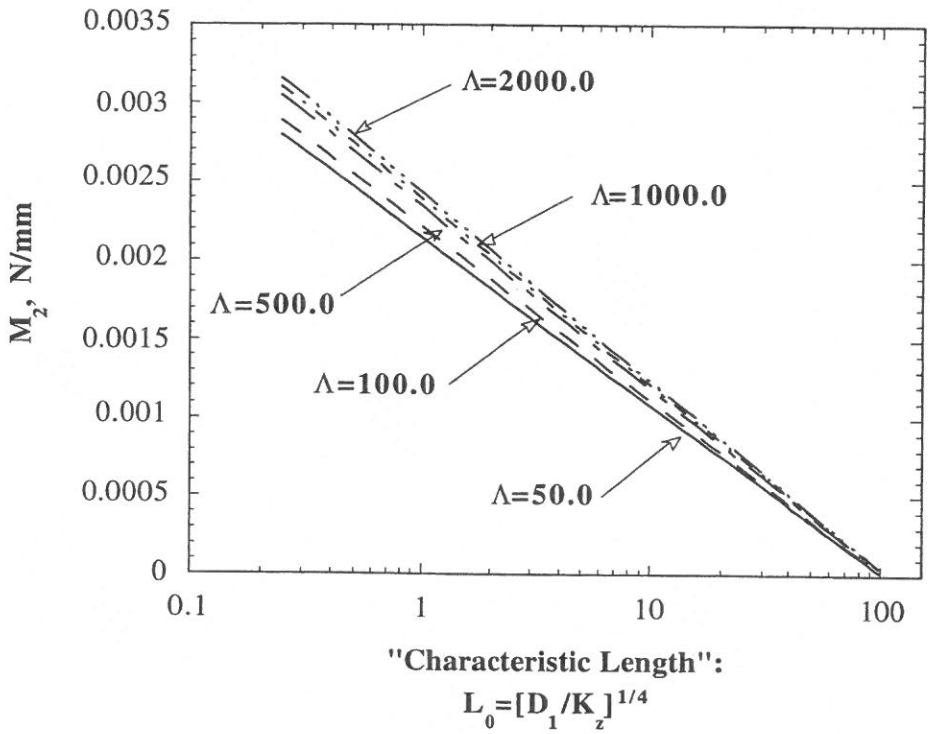

Fig. 25. Peak bending moment resultant M_2 in face-laminate 2 vs. L_0 and Λ (D_2/D_1=0.05). External load: $N_1(x=0)$=-P=-1.0 N/mm (unit load).

However, the most interesting new feature displayed by the plots in Figs. 25 and 26, is the influence of the adhesive/core-stiffness ratio Λ on the peak values of M_1, M_2.

Considering the results shown in Fig. 25, it is apparent that increasing the adhesive/core-stiffness ratio affects the bending state in face-laminate 1 such that the peak value of M_1 increases (absolute value) as well. Even though this effect is not very dramatic (displayed by the use of a linear scaled "Y-axis"), it is clear that an increase of $(M_1)_{peak}$ means an increase of the bending stresses in face-laminate 1. Thus, it is seen that the influence of Λ on the bending stress state in face-laminate 1 is similar to the influence exerted on the adhesive/resin layer and the core stress states.

All the observations derived from Fig. 25 about the relationship between the adhesive/core-stiffness ratio Λ and the peak value of M_1 are valid for the results displayed in Fig. 26 showing the M_2-Λ relationship. Thus, no additional comments will be given with respect to the results shown in Fig. 26.

To conclude this section, it has been demonstrated that the adhesive/resin layer, the core as well as the face-laminate stress states are strongly influenced by the adhesive/core-stiffness ratio Λ (and of course by L_0).The overall conclusion drawn is that the larger the value of Λ ,i.e., the larger the difference between the effective adhesive/resin layer stiffness (E_a/t_a) and the core stiffness K_z, the more severe stress concentrations are encountered.

8.3 "Secondary" parametric effects

The parametric study given in the two preceding sections illustrates the influence of what could be called the "primary parameters" (L_0, D_2/D_1 and Λ), thus indicating that these parameters exert primary influence on the local bending behaviour. This, of course, indicates that there are other, and less influential, parameters which also exerts influence on the local bending problem. These parameters could be called "secondary parameters", and their influence is at least partly included in the "primary parameters".
Examples of "secondary parameters" are: laminate extensional stiffnesses, laminate stacking sequences, laminate thicknesses, as well as laminate coupling effects (due to unsymmetric and unbalanced laminate lay-ups). The influence of these parameters will not be given any further attention in this report, but they will of course have to be considered in a design situation.

9.0 "HIGH-LIGHTING" OF PRIMARY DIFFERENCES BETWEEN TAPERED CFRP-SANDWICH AND UNSUPPORTED TAPERED CFRP-LAMINATE CASES

In the two examples presented in paragraphs 6.1 and 6.2 of this report, the differences between the local mechanical response encountered in tapered CFRP-sandwich panels and tapered unsupported CFRP-laminates (i.e. CFRP-laminates which are not acting as face-sheets of sandwich panels) were discussed. For the CFRP-sandwich case it was found, that the core material acts as a very efficient restraint on the lateral displacements, but as the face-laminate/core interaction at the same time imposes a short wave-length deflectional pattern, the resulting elastic

response differs significantly from the unsupported CFRP-laminate case. Especially three important differences were found:

- severe stress concentrations are induced in the core material in the sandwich case (obviously, for the unsupported case no core stresses exists as there is no supporting core-material);
- the adhesive/resin layer stress concentrations induced in the sandwich case tends to be more severe than in the unsupported case;
- The bending moment concentrations (and thereby the laminate bending stresses) concentrations found for the unsupported case are generally more severe than for the sandwich case.

The points made are quite important, as the temptation to analyse the tapered CFRP-sandwich problem with the well-known methods developed for the unsupported bonded "doubler"-problem is very nearby. As observed, however, this will neglect the existence of core transverse normal as well as shear stresses, it will underestimate the stress concentrations in the adhesive/resin layer which separates the base-line and reinforcing laminates, and finally it will overestimate the magnitude of the locally induced bending stresses in the base-line laminate (this at least being conservative).

In order to elaborate a bit on the latter two of the differences mentioned, the results of an additional (and small) parametric study will be given. The idea of the study is to give a quantitative impression of the differences between the peak adhesive/resin layer stresses, and the peak bending moment resultants encountered in tapered CFRP face-laminates of sandwich panels and unsupported CFRP-laminates, respectively. In the parametric study a thickness drop-off zone with the following characteristics is considered:

- a **reinforcing laminate** (face 2) made from 2 plies of HTS carbon fibre/ epoxy prepreg (same as face 2 in examples 1, 2 of sections 6.1 and 6.2) with stacking sequence $[\pm 45^\circ]$ and thickness t_2=0.1 mm is dropped (see section 6.1 for elastic properties).

- the **base-line laminate** (face 1) is assumed to be some "fictive" carbon-fibre laminate (made of UD-ply prepregs; unspecified stacking sequence) where the thickness is varied between t_1=0.2 mm and t_1=2.0 mm (the interesting thickness-range for most aerospace applications), and where the in-plane elastic properties are assumed to be as follows (values are representative for carbon-fibre/epoxy laminates with a "high" percentage of 0°-plies):
  E_{11}=65.0 GPa, E_{22}=8.0 GPa, ν_{12}=0.175, ν_{21}=1.35, G_{12}=16.0 GPa.

- the **core material** is assumed to be HEXCEL Al-honeycomb; 3/16"-5056-0.0007" which was specified in examples 1 and 2 of sections 6.1, 6.2.

- the **adhesive/resin layer** is assumed to the same as specified in examples 1 and 2 of sections 6.1, 6.2.

The results of the paramatric study are shown in Fig. 27 and 28. It should be noted here, that the quantitative results displayed are only strictly valid for the specific thickness drop-off configurations considered, and that all other configurations will yield different stress and moment resultant concentration values. However, the overall (qualitative) tendencies displayed are generally valid.

Fig. 27 shows the peak values of the normalised transverse normal and shear stress components, $(\sigma_a/\sigma_N)_{peak}$ and $(\tau_a/\sigma_N)_{peak}$, as functions of the thickness t_1 of the base-line laminate for the sandwich and unsupported CFRP-laminates, respectively.
Fig. 28 shows the corresponding peak values of the face-laminate bending moment resultants $(M_1)_{peak}$ as function of t_1 encountered for the sandwich and unsupported CFRP-laminates, respectively.

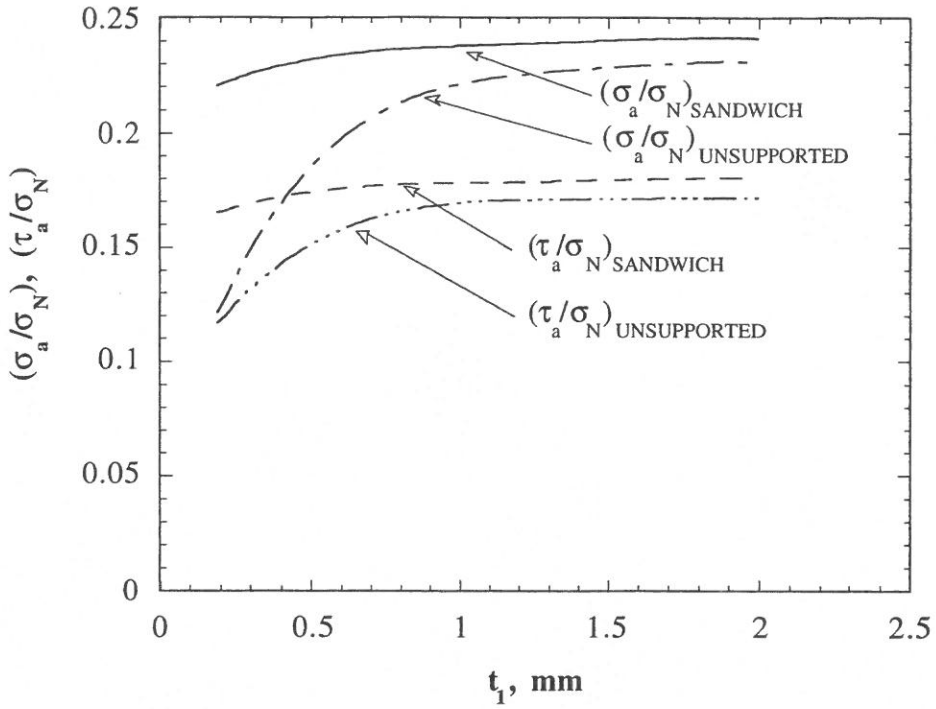

Fig. 27. $(\sigma_a/\sigma_N)_{peak}$ and $(\tau_a/\sigma_N)_{peak}$ vs. t_1 (0.2 mm $\leq t_1 \leq$ 2.0 mm) for sandwich and unsupported CFRP-laminates. The thickness of the reinforcing laminate is kept constant: t_2=0.1 mm (corresponding to 2 HTS carbon/epoxy plies).

Considering the results displayed in Fig. 27, it is observed that the adhesive/resin layer stress level is generally higher (as stated earlier) in the sandwich CFRP-laminates than in the unsupported CFRP-laminates. Furthermore, it is seen that this general observation is especially pronounced for small values of t_1 (which corresponds to small values of the elastic wave-length λ for the CFRP-sandwich case), while the difference between the adhesive/resin layer stress concentrations for the two cases decreases with increasing values of t_1.
Comparing the overall tendencies displayed in Fig. 27 (CFRP-sandwich results) with Figs. 17, 18 (section 8.1) and Figs. 22, 23 (section 8.2), some surprising and at first sight contradictory results shows. In Fig. 27 is it seen that $(\sigma_a/\sigma_N)_{peak}$ and $(\tau_a/\sigma_N)_{peak}$ increases with increasing values of t_1. Increasing values of t_1 corresponds to increasing values of the primary bending stiffness D_1 (assuming constant material properties), which again corresponds to increasing values of the elastic wave-length λ (also assuming constant K_z). Thus, in Fig. 27 it is seen that $(\sigma_a/\sigma_N)_{peak}$ and $(\tau_a/\sigma_N)_{peak}$

increases with increasing values of λ, while the opposite conclusion can be drawn from the results displayed in Figs. 17, 18, 22 and 23.
Another (and similar) apparent discrepancy between the results of Fig. 27 and the results of Figs. 17 and 18 can be found. In Fig. 27, $(\sigma_a/\sigma_N)_{peak}$ and $(\tau_a/\sigma_N)_{peak}$ increases with increasing values of t_1 (corresponding to increasing values of D_1), and as t_2 has been kept fixed (i.e. D_2 = constant), it is seen that the adhesive/resin peak stresses increases with decreasing values of the stiffness ratio D_2/D_1 (D_2 = constant and D_1 increasing). This result is completely opposite to the results displayed in Fig. 17 and 18.
The reason for these apparently contradictory results is not an inconsistency in the modelling of the thickness drop-off problem (fortunately), but is a consequence of the different circumstances (basic assumptions) under which the parametric study results displayed in sections 8.1, 8.2 and this section have been obtained.

One of the primary objectives of the parametric studies displayed in sections 8.1 and 8.2 were to show the relationship between the stress/moment concentrations and the "primary" parameter L_0 (characteristic length; see eq. (14)). The parameter L_0 is determined by D_1 and K_z, which imply that L_0 is determined by the "effective in-plane face-laminate E-modulus" ("E_{11}" for face-laminate 1), the face-laminate thickness t_1, and the core stiffness E_c. In order to facilitate the conduction of the parametric study results presented in sections 8.1 and 8.2 the face-thicknesses t_1 and t_2 as well as the core E-modulus E_c were treated as constants, while the "effective in-plane laminate E-moduli" of the face-laminates were treated as variables.
The parametric results displayed in Fig. 27, however, were obtained by varying t_1 with constant values of E_c and t_2 as well as the "in-plane effective E-moduli" of the face-laminates. The solution-procedure "runs" were conducted by specifying a unit compressive line load $N_1(x=0)=-P=-1.0$ N/mm, and it is readily seen that the value of the nominal stress σ_N decreases with increasing t_1 (as $\sigma_N = N_1(x=0)/t_1 = (-1.0$ N/mm$)/t_1$). When t_1 is increased (while t_2 is maintained constant), a smaller and smaller portion of the total load is transferred into the reinforcing laminate, and this causes the absolute value of the adhesive/resin stresses to decrease. This decrease is, however (as explained above), accompanied by a decrease in σ_N, and as the decrease of σ_N is more steep than the decrease of σ_a and τ_a (absolute values), the result displayed in Fig. 27 is that $(\sigma_a/\sigma_N)_{peak}$ and $(\tau_a/\sigma_N)_{peak}$ increases with increasing values of t_1.
Thus, the tendency of increasing values of normalised adhesive/resin stresses with increasing value of t_1 (corresponding to increasing value of the elastic wave-length λ and decreasing value of the stiffness ratio D_2/D_1) displayed in Fig. 27, can be attributed to the circumstances that the load-sharing between the two face-laminates, as well as the nominal stress (with which the adhesive stresses are normalised), changes in the conducted parametric study. This again shows, that proper interpretation of the parametric results is not a straight forward matter, and that it can be difficult to separate the effects of the various parameters influencing the mechanics of the thickness drop-off problem.

The results displayed in Fig. 28, showing the absolute values of the peak bending moment resultants for the sandwich and the unsupported tapered CFRP-laminate cases as functions of t_1. These peak bending moment resultants occurs in face-laminate 1, and for the sandwich case, $(M_1)_{peak}$ is negative (for compressive external load) and is located at $x \approx L_1$ (see Fig. 10), whereas for the unsupported case, $(M_1)_{peak}$ is positive and occurs for $x > L_1$ (see Fig. 15).

It is seen from Fig. 28, that the peak bending moment resultant values for both cases increases with increasing values of t_1. Furthermore, it is seen that $|(M_1)_{peak}|$ tends to be larger for the unsupported case than for the sandwich CFRP-laminate case. The difference between values of $|(M_1)_{peak}|$-values is smallest for small values of t_1, and increases with increasing t_1.
For $t_1>0.8$ mm, the relative difference between the two cases is almost constant, and, moreover, the continued increase of the peak bending moment resultant values with increasing t_1 has almost vanished (i.e., $|(M_1)_{peak}|_{\text{UNSUPPORTED}} \approx 2\ |(M_1)_{peak}|_{\text{SANDWICH}} \approx$ constant).
The tendency of increasing values of $|(M_1)_{peak}|$ with increasing values of t_1 (which corresponds to increasing λ–value and decreasing D_2/D_1-ratio) observed from Fig. 28, is apparently a complete contradiction to the results displayed in Figs. 20 and 25 of sections 8.1-8.2 (same type of "discrepancy" as observed for the results shown in Fig. 27). As before, this "apparent" discrepancy can be attributed to the mere fact that the circumstances under which the parametric study results shown in Fig. 28 have been obtained are different from the circumstances under which the results shown in sections 8.1 and 8.2 were obtained.

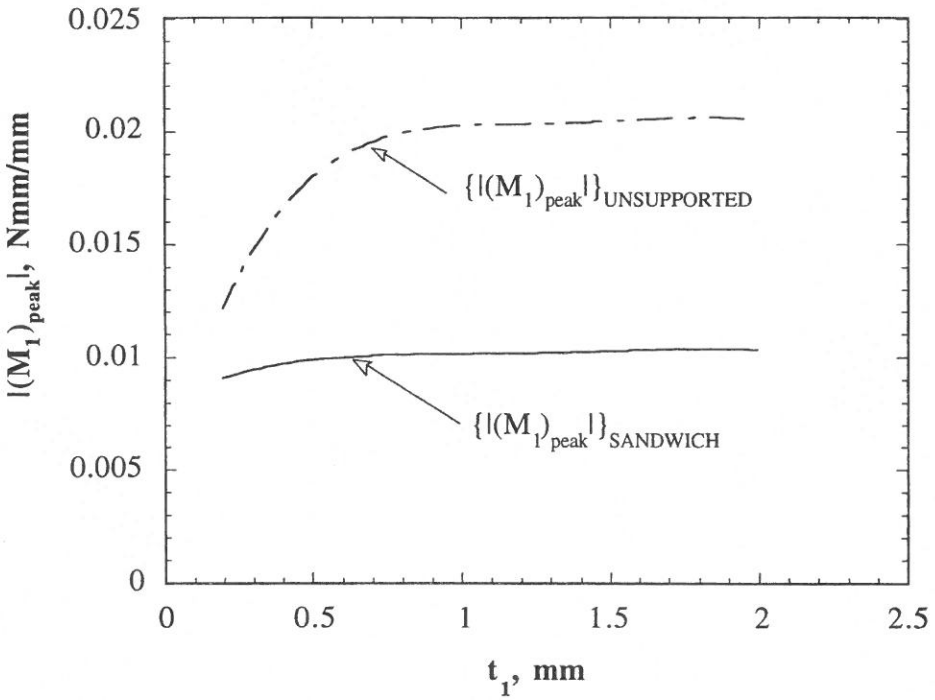

Fig. 28. $|(M_1)_{peak}|$ vs. t_1 (0.2 mm $\leq t_1 \leq$ 2.0 mm) for sandwich and unsupported CFRP-laminates. The thickness of the reinforcing laminate is kept constant: t_2=0.1 mm (corresponding to 2 HTS carbon/epoxy plies).

Thus, the reason for $|(M_1)_{peak}|$ to increase with increasing t_1 in Fig. 28 (not very pronounced for the sandwich case) is, that the increase of t_1 causes the bending stiffness D_1 to increase ($D_1 \propto t_1^3$), and even though the curvature $\beta_1'=-w_1''$ of face-laminate 1 decreases due to the increased bending stiffness (note that $M_1=D_1\ \beta_1'$), the product between D_1 and β_1' increases overall. This tendency is especially pronounced for 0.2 mm $\leq t_1 \leq$ 0.8 mm for the unsupported CFRP-laminate case.

10. DESIGN GUIDELINES

Based on the results presented in chapters 6, 8 and 9, it is possible to formulate a number of simple design guidelines for tapering face-laminates of CFRP-sandwich panels:

- The thickness drop-off step-size should be made as small as possible in order to minimise the parameter D_2/D_1. If possible, the drop-off step-size should be limited to a thickness of two ply-thicknesses (one ply-thickness being impractical and unrealistic).
- As a direct continuation of the first design guideline, a strong advise is given to avoid dropping a thick sub-laminate (reinforcement) containing a large number of plies abruptly. It is preferable to drop a large number of plies as a number of thin sub-laminates evenly distributed over a some longitudinal distance.
- The spacing between two adjacent thickness drop-offs should at least equal the wave-length of the core/face-laminate elastic response: $\lambda=2\pi L_0$ (and preferably it should exceed λ).
- If possible, the adhesive/resin properties as compared to the core properties should be chosen in such a way as to minimise the adhesive/core-stiffness ratio $\Lambda=(E_a/t_a)/K_z$.
- Finally, as significant stress concentrations in the adhesive/resin layer interfacing the base laminate and the reinforcing laminate are unavoidable, an adhesive/resin system with long elongation to failure capability (ductility) should be used.

The simple guidelines formulated above agrees very well with the general design guidelines specified for unsupported CFRP-composites in refs. [7], [8].

11. FINAL COMMENTS, CONCLUSIONS AND SUGGESTIONS FOR AN EXPERIMENTAL STUDY

A mechanical model of the thickness drop-off problem encountered in CFRP-faced sandwich panels has been developed, and it has been shown that the inclusion of core/face-laminate interaction in the model is of paramount importance. This has been achieved by introducing a two-parameter elastic foundation model, which includes the shearing interaction between the core material and the face-laminates.
The model presented has been restricted to considering the face-laminates as layered linear elastic beam-elements, or layered linear elastic orthotropic plate-elements in cylindrical bending, and the results presented therefore have to be evaluated in this context. Furthermore, linear elastic assumptions have been used for the core material and the resin/adhesive layer interfacing the base-line and reinforcing face-laminates.

The actual problem solution has been accomplished by transforming the resulting multiple-point boundary value problem into a series of interconnected initial value problems, which can be solved using a direct integration scheme. The method used, known as the "multi-segment method of integration", was implemented on a HP-workstation using the mathematical software-package MATLAB® (version 4.1), and the numerical solution procedure developed has proven to be very efficient and robust.

The numerical solution procedure developed has been used for conducting a series of parametric studies, and three "primary parameters" were found to exert significant influence on the stress concentrations induced by local bending in the adhesive/resin layer, the core material and the face-laminates. The three "primary parameters" are:

- the characteristic length of face-laminate 1: $L_0 = \sqrt[4]{\frac{D_1}{K_z}}$.
- the ratio of the bending stiffness of face-laminate 2 (reinforcement) to the bending stiffness of face-laminate 1 (base-line laminate): $\frac{D_2}{D_1}$.
- the ratio of the adhesive/resin layer stiffness (E_a/t_a) to the transverse foundation modulus K_z (core stiffness): $\Lambda = \frac{(E_a / t_a)}{K_z}$.

It was found that an increase of all the quoted parameters was accompanied by significantly increased stress concentrations.

As mentioned in the introductory chapters of this report, the solution method developed (beam/plate model) should be looked upon as the simplest possible version of a general beam/plate/shell model of the thickness drop-off problem. However, it would be rather simple to implement a number of additional features such as:

- Using **higher-order beam/plate/shell theory** in order to account for the transverse shearing effects. This feature might be valuable/necessary in cases where thick (substantial number of plies) face-laminates are used.

- Expanding the model to **general rotationally symmetric shells** (cylinders or shells with arbitrary meridian shapes). The material properties of the face-laminates can be modelled as generally orthotropic (i.e., the principal material directions do not have to coincide with the principal directions of curvature), and the external loading can be non-axisymmetric.

- **Non-linear material behaviour** of the adhesive/resin layer, the face-laminates and the core material can be included in the modelling by adopting an incremental formulation. This additional feature (at least including non-linear adhesive/resin and/or core properties) would be necessary in order to enable the prediction of the failure load and the actual failure mode.

- **Geometrically non-linear effects** can also be included in the model by adopting a non-linear strain-displacement relationship together with an incremental formulation.

The work reported so far has been solely theoretical, and even though not much doubt can be raised towards the quality of the predictions in a qualitative sense, an evaluation of the actual quantitative predictions of the model would be highly desirable. Thus, an experimental investigation with the objective of verifying/adjusting the model is currently being considered.
No decision has been made regarding the experimental technique to be used, but two types of techniques are being considered:

1. **Strain gauge measurement** of surface strains on the tapered face-laminates of CFRP-sandwich panels.
   In order to carry out such an experimental investigation successfully, it would be of paramount importance that the wave-lengths of the elastic deformations should be sufficiently large to enable the measurement of the surface strains close to the thickness drop-off areas. In order to accomplish this, CFRP-sandwich panels with rather thick laminates should be used in the experiments.

Suitable geometrical and material properties for the test-specimens could, of course, be determined by use of the developed solution procedure.

2. **Optical measurement** of the displacement field of the surface of the tapered face-laminates of CFRP-sandwich panels.
For the present investigation, optical measurement of the displacement field can be accomplished by two different methods: **holographic interferometry** (double exposure or real-time), or **moiré fringe interferometry**. The former method is about one order of magnitude more sensitive than the latter, as the smallest measurable displacement using holographic interferometry is about $1\text{-}2\times10^{-4}$ mm, whereas it is about $2\text{-}3\times10^{-3}$ mm using moiré fringe interferometry. From this it is seen that the most promising method in the present context would be holographic interferometry, as the lateral deflections encountered locally will be very small.

REFERENCES

1. Thomsen, O. T., Analysis of local bending effects in sandwich plates with orthotropic face layers subjected to localised loads. *Composite Structures* **25** (1993) 511-520.
2. Vlasov, V. Z. & Leont'ev, N. N., *Beams, Plates and Shells on Elastic Foundations.* Moscow, 1960 (English translation by Israel Programme for Scientific Translation, Jerusalem, 1966).
3. Thomsen, O. T., Elasto-static and elasto-plastic stress analysis of adhesive bonded tubular lap joints, *Composite Structures* **21** (1992) 249-259.
4. Kalnins, A., Analysis of shells of revolution subjected to symmetrical and nonsymmetrical loads. *Transactions of the ASME, Journal of Applied Mechanics* **31** (September 1964) 467-476.
5. Thomsen, O. T., *Analysis of Adhesive Bonded Generally Orthotropic Circular Cylindrical Shells.* Ph.D.-thesis, Institute of Mechanical Engineering, Aalborg University, 1989.
6. Fokker Report No. TR-R-86-CSE-080, *Final Report of Composite Structural Element (CSE)*, November 1986.
7. Thomas, D.M. & Webber, J. P. H., A design-study into the delamination behaviour of tapered composites, *Composite Structures* **27** (1994) 379-388.
8. ESDU Data Item 91003, *Delamination of Tapered Composites.* ESDU International plc.. London, Nov. 1991.

APPENDICES: MATLAB® "M-FILES"

Appendix 1: EXEC.m (main execution program)

```
% M-file:  EXEC.m
%
% Solution of "thickness change" induced bending
% problem in CFRP-sandwich panels.

clear
clear global

% Loading of Input data; Calculation of foundation moduli and stiffness
% coefficients; Definition of B.C.'s through non-singular transformation
% matrices T0, T1 T2 and B.C.-vectors u01, u11, u23 and u24.

global N1 N2 fvar fhalf Nvar

Input;          % Using M-file: Input.m.
stiffcoeff;     % Using M-file: stiffcoeff.m.
BC;             % Using M-file BC.m.

% Solving the problem involves solution of a matrix equation of the form:
% [S]{U}={V} (U=S\V in MatLab syntax). The system matrix [S], the solution
% vector {U}, and the "load vector" {V} are defined by:

fvar=6;
fhalf=fvar/2;
Nvar=(N1+2*N2)*fvar;
S=sparse(Nvar,Nvar);                    % Creation of system matrix [S].
U=zeros(Nvar,1);                        % Creation of solution vector {U}.
V=zeros(Nvar,1);                        % Creation of "load vector" {V}.
V(Nvar-fvar+1:Nvar-fhalf,1)=u23;        % B.C.'s in last segment.
V(Nvar-fhalf+1:Nvar,1)=u24;             %       do.

% The structure of the system matrix [S] is roughly defined by:
%
% | P1  -|      "segment 1"                                              |
% | P2      -|  _ _ _ _ _ _                                             |
% |      Y1 Y2  -|     "segment 2 %                                      |
% |      Y3 Y4     -| _ _ _ _ _ _                                       |
% |                Y1 Y2  -|     "segment 3"              "REGION 1"   |
% |                Y3 Y4      -|  _ _ _ _ _ _                          |
% |                .                                                    |
% |                .                                                    |
% |   _ _ _ _ _ _    _____________________                               |
% |                  Y2  Y3  Y4     -|                                  |
% | "segment         Y6  Y7  Y8          -|          "REGION 2"         |
% |    N1+1"         Y10 Y11 Y12             -|                        |
```

```
% |  _ _ _ _ _ _     Y14 Y15 Y16                -I                          |
% |                  Y1  Y2  Y3  Y4    -I                                  |
% |   "segment N1+2" Y5  Y6  Y7  Y8      -I                                |
% |                  Y9  Y10 Y11 Y12         -I                           |
% |  _ _ _ _ _ _     Y13 Y14 Y15 Y16             -I                       |
% |                      .                                                 |
% |                      .                                                 |
% |                      _ _ _ _ _ _                                       |
% |                                     Y1  Y2  Y3  Y4   -I               |
% |          "segment N1+N2"            Y5  Y6  Y7  Y8       -I          |
% |                                     Y9  Y10 Y11 Y12                  |
% |                                     Y13 Y14 Y15 Y16                  |
%
% where the I's are (3,3)-unit matrices.
%
% REGION 1; SEGMENTS 1 TO N1:

I=-eye(N1*fvar,N1*fvar);
S(1:N1*fvar,fhalf+1:N1*fvar+fhalf)=I;
clear I;

% "step" goes from 1 to N1 in REGION 1, but 1. segment is special.

% 1. segment; REGION 1:
step=1;

Y_1=eye(fvar,fvar);          % Creation of (fvar*fvar)-matrix Y_1.
YY1=eye(fvar,fvar);
Y10=YY1(:);                  % Specification of initial conditions at x=0.
x0=0;
dx1=L1/N1;
x1=x0+dx1;
[x_1,Y1]=ode45('DDX_Y1',x0,x1,Y10);
[m,n]=size(Y1);
Y_1(:)=Y1(m,1:n);

% "Filling in" of "load vector {V}", and system matrix [S]:
YY=Y_1*inv(T0);
V(1:fhalf,1)=-YY(1:fhalf,1:fhalf)*u01;
V(fhalf+1:fvar,1)=-YY(fhalf+1:fvar,1:fhalf)*u01;
S(1:fvar,1:fhalf)=YY(1:fvar,fhalf+1:fvar);

% Stepping over segments 2 to N2 in REGION 1:
for step=2:N1
        J=(step-1)*fvar;
        S(J+1:J+fvar,J+1-fhalf:J+fhalf)=Y_1;     % "Filling in" of [S].
end;
% {V}=0 in these segments; "filled in" already.
```

```
% REGION 2; SEGMENTS N1+1 TO N1+N2:

dum=fvar*(2*N2-1);
I=-eye(dum,dum);
S(N1*fvar+1:N1*fvar+dum,(N1+1)*fvar+1:Nvar)=I;
clear I;clear dum;

% "step" goes from 1 to N2 in REGION 2, but 1. and last segments are
% special.

% REGION 2; segment 1 (N1+1):
step=1;

Y_2=eye(2*fvar,2*fvar);    % Creation of (2fvar*2fvar)-matrix Y_2.
YY2=eye(2*fvar,2*fvar);
Y20=YY2(:);                % Specification of initial conditions at x=L1.
x0=0;
dx2=L2/N2;
x1=x0+dx2;
[x_2,Y2]=ode45('DDX_Y2',x0,x1,Y20);
[p,q]=size(Y2);
Y_2(:)=Y2(p,1:q);

% "Filling in" of "load vector" {V}:
YY=Y_2*inv(T1);
V(N1*fvar+1:N1*fvar+fhalf,1)=-YY(1:fhalf,1:fhalf)*u11;
V(N1*fvar+fhalf+1:(N1+1)*fvar,1)=-YY(fhalf+1:fvar,1:fhalf)*u11;
V((N1+1)*fvar+1:(N1+1)*fvar+fhalf,1)=-YY(fvar+1:fvar+fhalf,1:fhalf)*u11;
V((N1+1)*fvar+fhalf+1:(N1+2)*fvar,1)=-YY(fvar+fhalf+1:2*fvar,1:fhalf)*u11;

% "Filling in" of system matrix [S]:
S(N1*fvar+1:(N1+2)*fvar,N1*fvar-
fhalf+1:(N1+1)*fvar)=YY(1:2*fvar,fhalf+1:2*fvar);
clear YY;

% Stepping over segments 2 to N2-1 in REGION 2:
for step=2:(N2-1)
        J=N1*fvar+(step-1)*2*fvar;
        S(J+1:J+2*fvar,J+1-fvar:J+fvar)=Y_2;
end;
% {V}=0 in these segments; "filled in" already.

% REGION 2; segment N2 (N1+N2):
step=N2;

% "Filling in" of system matrix [S]:
YY=T2*Y_2;
J=N1*fvar+(N2-1)*2*fvar;
S(J+1:J+2*fvar,J-fvar+1:J+fvar)=YY;
clear YY;
% {V} "filled in" already.
```

```
% After integration in each segment (1 to N1+N2), and after assembly
% of the system equations [S]{U}={V}, the solution is obtained as:
U=S\V;

% A small "repair job" on the solution vector {U} still remains,
% as {U} does not contain the prescribed B.C.'s u01 (x=0), u11 (x=L1),
% and u23, u24 (x=L1+L2).
% The final solution vector components are stored in the vector {Ures}:
Ures(1:fhalf,1)=u01;
Ures(fhalf+1:N1*fvar,1)=U(1:N1*fvar-fhalf,1);
Ures(N1*fvar+1:N1*fvar+fhalf,1)=u11;
Ures(N1*fvar+fhalf+1:fvar*(N1+2*N2+1),1)=U(N1*fvar-
fhalf+1:fvar*(N1+2*N2),1);
Ures(Nvar+fvar+1:Nvar+fvar+fhalf,1)=u23;
Ures(Nvar+fvar+fhalf+1:Nvar+2*fvar,1)=u24;

% The elements of {Ures} at the ends (x=0, x=L1+L2), and at the
% junction between REGIONS 1 and 2 (x=L1) still needs rearrangement:

Ures(1:fvar,1)=inv(T0)*Ures(1:fvar,1);
% x=0
Ures(N1*fvar+1:(N1+2)*fvar,1)=inv(T1)*Ures(N1*fvar+1:(N1+2)*fvar,1);
% x=L1
Ures(Nvar+1:Nvar+2*fvar,1)=inv(T2)*Ures(Nvar+1:Nvar+2*fvar,1);
% x=L1+L2


% Calculation of complete solution using M-file: STRESScalc.m:
STRESScalc;

% Calculation of "upper surface" strain fields using M-file: STRAIN.m:
STRAIN;

% "Separation" of lateral deflection components: w1, w2 as well
% as longitudinal displacement components u1, u2.
for i=1:N1*(m-1)+N2*(p-1)+1
        w1(i,1)=yy1(2,i);
        u1(i,1)=yy1(1,i);
end;
offset=2e-5; % Used for plot-"scaling" of deformed structure.
for i=1:N2*(p-1)+1
        w2(i,1)=yy2(2,i);
        w2plot(i,1)=w2(i,1)+offset*(0.5*(tf1+tf2)+ta);   % w2-comp. for
                                                         % DEFORM.m
        u2(i,1)=yy2(1,i);
end;

% Definition of x1- and x2-coordinates.
xco1(1:N1*(m-1)+1,1)=xco(1:N1*(m-1)+1,1);
xco2(1:N2*(p-1)+1,1)=xco(N1*(m-1)+1:N1*(m-1)+N2*(p-1)+1,1);
```

Appendix 2: Input.m (in-data for EXEC.m)

```
% M-file: Input.m
%
% Input data for "thickness change"-problem

% face layer no. 1 (base-line laminate):
load LAMinput1.dat;        % loading laminate properties from ASCII-file.
LI=LAMinput1;
[R,C]=size(LI);
LAMINATE;          % calculating laminate stiffness properties; CLT-method.
A1=a11;            % "principal" extensional stiffness.
Df1=d11;           % "principal" bending stiffness.
tf1=t;             % laminate thickness.
L1=100;            % length of REGION 1.
N1=10;             % number of segments in REGION 1 (NB: minimum 3)

% face layer no. 2 (reinforcment):
load LAMinput2.dat;        % loading laminate properties from ASCII-file.
LI=LAMinput2;
[R,C]=size(LI);
LAMINATE;          % calculating laminate stiffness properties; CLT-method.
A2=a11;            % "principal" extensional stiffness.
Df2=d11;           % "principal" bending stiffness.
tf2=t;             % laminate thickness.
L2=100;            % length of REGION 2
N2=15;             % number of segments in REGION 2 (NB: minimum 3).

% Adhesive layer:
Ea=2500;                   % E-modulus.
nya=0.40;                  % Poisson's ratio.
ta=0.01;
Eaeff=Ea*(1-nya)/((1-2*nya)*(1+nya));  % effective adhesive E-modulus;
                                       % Eaeff>Ea.
Ga=Ea/(2*(1+nya));         % G-modulus.

% Honeycomb core material (Hexagonal cells, Al.):
Ec=500;                    % E-modulus.
nyc=0.3;                   % Poisson's ratio.
c=10;                      % core height.

% Calculation of effective core stiffness and foundation moduli:
E0=Ec/(1-nyc^2);   % effective Young's modulus.
ny0=nyc/(1-nyc);   % effective Poisson's ratio.
gamma=1.5;         % impirical factor.
phi=2*gamma*c;
psi1=(sinh(phi)*cosh(phi)+phi)/((sinh(phi))^2);
psi2=(sinh(phi)*cosh(phi)-phi)/((sinh(phi))^2);
Kx1=psi2*E0/(4*(tf1*c*gamma*(1+ny0)));     % foundation modulus - shear;
                                           % region 1.
Kx2=Kx1*tf1/(tf1+ta+tf2);                  % foundation modulus - shear;
```

```
                                        % region 2.
Kz=psi1*gamma*E0/(1-ny0^2);             % foundation modulus -
                                        % transverse normal

% External inplane loading:
P=-1;


% PARAMETRIC STUDY 1: var. of L0 and D2/D1:

% L0=10;            % variable: L0=0.25, 0.5, 1.0, 10.0, 100.0
% L1=15*L0;         % HINT:  min. 10*L0
% N1=60;
% L2=L1;            % HINT:  min. 10*L0
% N2=90;
% Df1=L0^4*Kz;
% koef=1.0;         % variable: koef=D2/D1=0.01, 0.05, 0.1, 0.5, 1.0
% Df2=koef*Df1;
% tf1=0.5;tf2=0.5;
% A1=Df1*12/(tf1^2);
% A2=Df2*12/(tf2^2);


% PARAMETRIC STUDY 2: var. of L0 and (Ea/ta)/Kz:

 % L0=1;            % variable: L0=0.25, 0.5, 1.0, 10.0, 100.0
% L1=15*L0;         % HINT:  L1 min. 10*L0
% N1=40;
% L2=L1;            % HINT:  L2 min. 10*L0
% N2=80;
% Df1=L0^4*Kz;
% Df2=0.05*Df1;

% tf1=0.5;tf2=0.5;
% A1=Df1*12/(tf1^2);
% A2=Df2*12/(tf2^2);
% koef=250.0;       % variable: koef=(Ea/ta)/Kz=50, 100, 500, 1000, 2000
                    %Ea=koef*Kz*ta;
% Eaeff=Ea*(1-nya)/((1-2*nya)*(1+nya));     % effective adhesive Youngs
                                            % modulus, Eaeff>Ea
% Ga=Ea/(2*(1+nya));
```

Appendix 3: LAMINATE.m (calculation of laminate stiffnesses; used by Input.m)

```
% M-file:  LAMINATE.m
%
% "LAMINATE" calculates laminate stiffnesses from the stiffness coefficients
```

```
%  of  the individual plies.
% "LAMINATE" is based on classical laminate theory: CLT-theory.

% The input for "LAMINATE" should be specified in the form:
% "ply 1"(counted from the bottom): E11  E22  nu12  G12 h  theta
% "ply 2":              .....
% ....
% "ply R":              .....

t=0;    % intialising.

% Calculation of laminae-stiffnesses from
% engineering constants E11, E22, vu12, G12, h, theta.
for i=1:R
        t=t+LI(i,5);
        theta=LI(i,6)*pi/180;
        si2=(sin(theta))^2;
        co2=(cos(theta))^2;
        si4=(si2)^2;
        co4=(co2)^2;
        si2co2=si2*co2;

        dum=LI(i,3)*LI(i,2)/LI(i,1);
        dum=1-LI(i,3)*dum;
        q11=LI(i,1)/dum;
        q22=LI(i,2)/dum;
        q12=LI(i,3)*LI(i,2)/dum;
        q66=LI(i,4);

        Q11(i)=q11*co4+2*(q12+2*q66)*si2co2+q22*si4;
        Q22(i)=q11*si4+2*(q12+2*q66)*si2co2+q22*co4;
        Q12(i)=(q11+q22-4*q66)*si2co2+q12*(co4+si4);
        Q66(i)=(q11+q22-2*(q12+q66))*si2co2+q66*(co4+si4);
end;

a11=0;a12=0;a22=0;a66=0;      % "initialising".
b11=0;b12=0;b22=0;b66=0;
d11=0;d12=0;d22=0;d66=0;

tu=-t/2;        % "starting point for stepping over laminate thickness".

for i=1:R
        tu=tu+LI(i,5);
        tb=tu-LI(i,5);

        % Extensional stiffnesses - "A-matrix".
        a11=a11+Q11(i)*LI(i,5);
        a12=a12+Q12(i)*LI(i,5);
        a22=a22+Q22(i)*LI(i,5);
        a66=a66+Q66(i)*LI(i,5);
```

```
        % Coupling stiffnesses - "B-matrix".
        b11=b11+0.5*Q11(i)*(tu^2-tb^2);
        b12=b12+0.5*Q12(i)*(tu^2-tb^2);
        b22=b22+0.5*Q22(i)*(tu^2-tb^2);
        b66=b66+0.5*Q66(i)*(tu^2-tb^2);

        % Bending stiffnesses - "D-matrix".
        d11=d11+Q11(i)*(tu^3-tb^3)/3;
        d12=d12+Q12(i)*(tu^3-tb^3)/3;
        d22=d22+Q22(i)*(tu^3-tb^3)/3;
        d66=d66+Q66(i)*(tu^3-tb^3)/3;
end;
```

Appendix 4: LAMinput1.dat (input file for LAMINATE.m containing material data for face-laminate 1)

Example of contents of LAMinput1.dat (corresponding to example 1 in section 6.1: 5-ply HTS-carbon fibre/epoxy laminate):

```
115000    7100    0.3    4000    0.05    25
115000    7100    0.3    4000    0.05    -25
115000    7100    0.3    4000    0.05    0
115000    7100    0.3    4000    0.05    -25
115000    7100    0.3    4000    0.05    25
```

Appendix 5: LAMinput2.dat (input file for LAMINATE.m containing material data for face-laminate 2)

Example of contents of LAMinput2.dat (corresponding to example 1 in section 6.1: 2-ply HTS-carbon fibre/epoxy laminate):

```
115000    7100    0.3    4000    0.05    45
115000    7100    0.3    4000    0.05    -45
```

Appendix 6: stiffcoeff.m (calculation of stiffness coefficients for system equations; used by EXEC.m)

```
% M-file: stiffcoeff.m
%
% Calculation of STIFFNESS COEFFICIENTS contained in STIFFNESS
% MATRICES of system of governing equations in REGION 1  &  REGION 2

% REGION 1:
```

```
global a14 a23 a35 a41 a43 a51 a53 a56 a62

a14=1/A1;
a23=-1;
a35=1/Df1;
a41=0;
a43=-Kx1*tf1*0.5;
a51=0;
a53=-a43*0.5*tf1;
a56=1;
a62=Kz;


% REGION 2:

global b14 b23 b35 b41 b43 b47 b49 b51 b53 b56 b57 b59
global b62 b68 b710 b89 b911 b101 b103 b107 b109 b111
global b113 b117 b119 b1112 b122 b128

b14=a14;

b23=-1;

b35=a35;

b41=Ga/ta;
b43=0.5*tf1*(-Kx2+Ga/ta);
b47=-Ga/ta;
b49=-b47*0.5*tf2;

b51=0.5*(tf1+ta)*Ga/ta;
b53=0.25*tf1*(Kx2*tf1+(tf1+ta)*Ga/ta);
b56=1;
b57=-0.5*(tf1+ta)*Ga/ta;
b59=-b57*tf2*0.5;

b62=Kz+Eaeff/ta;
b68=-Eaeff/ta;

b710=1/A2;

b89=-1;

b911=1/Df2;

b101=b47;
b103=b47*tf1*0.5;
b107=-b47;
b109=b47*tf2*0.5;

b111=-b47*0.5*(tf2+ta);
```

```
b113=b111*0.5*tf1;
b117=-b111;
b119=b111*0.5*tf2;
b1112=1;

b122=b68;
b128=-b68;
```

Appendix 7: BC.m (specification of boundary conditions; used by EXEC.m)

```
% M-file: BC.m
%
% Definition/Specification of B.C.'s through non-singular transformation
% matrices T0, T1, T2 and associated B.C. vectors u01, u11, and u23, u24.

% MATRIX T0 & VECTOR u01: "Simple support: x=0 (face-laminate 1)".
TT0=zeros(6,6);
TT0(1,2)=1;
TT0(2,4)=1;
TT0(3,5)=1;
TT0(4,1)=1;
TT0(5,3)=1;
TT0(6,6)=1;
T0=sparse(TT0);    % Sparse matrix storage.
u01=[0 P 0]';

% MATRIX T1 & VECTOR u11: "Free edge: x=L1 (face-laminate 2)".
TT1=zeros(12,12);
TT1(1,10)=1;
TT1(2,11)=1;
TT1(3,12)=1;
TT1(4,1)=1;
TT1(5,2)=1;
TT1(6,3)=1;
TT1(7,4)=1;
TT1(8,5)=1;
TT1(9,6)=1;
TT1(10,7)=1;
TT1(11,8)=1;
TT1(12,9)=1;
T1=sparse(TT1);    % Sparse matrix storage.
u11=[0 0 0]';

% MATRIX T2 & VECTORS u23, u24: "Symmetry condition: x=L1+L2 (face-
% laminates 1+2)".
TT2=zeros(12,12);
TT2(1,2)=1;
TT2(2,4)=1;
```

```
TT2(3,5)=1;
TT2(4,8)=1;
TT2(5,10)=1;
TT2(6,11)=1;
TT2(7,1)=1;
TT2(8,3)=1;
TT2(9,6)=1;
TT2(10,7)=1;
TT2(11,9)=1;
TT2(12,12)=1;
T2=sparse(TT2);    % sparse matrix storage.
u23=[0 0 0]';
u24=[0 0 0]';
```

Appendix 8: DDX_Y1.m (derivation of set of 36 1.order ordinary differential equations in region 1; used by EXEC.m)

```
% M-file: DDX_Y1.m

function Y1dot = DDX_Y1(x,Y1)
% DDX_Y1(x,Y1) returns the state derivatives of the beam/plate/shell
% equations in REGION 1; i.e. 36 coupled first order ODE's.
% Used by ode45.

global a14 a23 a35 a41 a43 a51 a53 a56 a62

A(6,6)=0;          % create 6*6 matrix A.
A(1,4)=a14;
A(2,3)=a23;
A(3,5)=a35;
A(4,1)=a41;
A(4,3)=a43;
A(5,1)=a51;
A(5,3)=a53;
A(5,6)=a56;
A(6,2)=a62;

yt1(6,6)=0;   % create a 6*6 matrix yt1.
yt1(:)=Y1;    % copy vector Y1 into yt1, columnwise.
yt1=A*yt1;
Y1dot(:)=yt1;
```

Appendix 9: DDX_Y2.m (derivation of set of 144 1.order ordinary differential equations in region 2; used by EXEC.m)

```
% M-file: DDX_Y2.m
%
function Y2dot = DDY_Y2(x,Y2)
% DDX_Y2(x,Y2) returns the state derivatives of the beam/plate/shell
% equations in REGION 2; i.e. 144 coupled first order ODE's.
% Used by ode45.

global b14 b23 b35  b41 b43 b47 b49 b51 b53 b56 b57
global b59 b62 b68 b710 b89 b911 b101 b103 b107 b109
global b111 b113 b117 b119 b1112 b122 b128

B(12,12)=0;          % create 12*12 matrix B.
B(1,4)=b14;

B(2,3)=b23;

B(3,5)=b35;

B(4,1)=b41;
B(4,3)=b43;
B(4,7)=b47;
B(4,9)=b49;

B(5,1)=b51;
B(5,3)=b53;
B(5,6)=b56;
B(5,7)=b57;
B(5,9)=b59;

B(6,2)=b62;
B(6,8)=b68;

B(7,10)=b710;

B(8,9)=b89;

B(9,11)=b911;

B(10,1)=b101;
B(10,3)=b103;
B(10,7)=b107;
B(10,9)=b109;

B(11,1)=b111;
B(11,3)=b113;
B(11,7)=b117;
B(11,9)=b119;
```

```
B(11,12)=b1112;

B(12,2)=b122;
B(12,8)=b128;

yt2(12,12)=0;        % create a 12*12 matrix.
yt2(:)=Y2;           % copy vector Y2 into yt2, columnwise.
yt2=B*yt2;
Y2dot(:)=yt2;
```

Appendix 10: STRESScalc.m (calculation of adhesive/resin layer stresses, core stresses as well as face-laminate normal stress, bending moment and transverse shear stress resultants; used by EXEC.m)

```
% M-file: STRESScalc.m
%
% DERIVATION OF COMPLETE SOLUTION:
% Foundation stress components; Adhesive/Resin-layer stress components;
% Stress and Moment resultants for face-laminates 1 and 2.

global fvar fhalf Nvar N1 N2 n m p q Y1 Y2 dx1 dx2 Ures
global sc tc sa ta Nx1 Nx2 Mx1 Mx2 Qx1 Qx2

% REGION 1; segments 1 to N1.
% Stepping over segments 1 to N1:
Y(fvar,fvar)=0;       % creation of fvar*fvar matrix Y.
for step=1:N1
      J1=(step-1)*fvar;
      for i=1:m-1
            J2=(step-1)*(m-1)+i;
            Y(:)=Y1(i,1:n);
            yy1(1:fvar,J2)=Y*Ures(J1+1:J1+fvar,1);        % FACE 1
                                                          % sol. vectors.
            sc(J2,1)=Kz*yy1(2,J2);                % Found. transv. normal
                                                  % stress.
            tc(J2,1)=-Kx1*0.5*tf1*yy1(3,J2);      % Found. shear stress.

            Nx1(J2,1)=yy1(4,J2);      % Normal stress result.; FACE 1.
            Mx1(J2,1)=yy1(5,J2);      % Bending moment result. FACE 1.
            Qx1(J2,1)=yy1(6,J2);      % Trans. shear str. result.; FACE 1.

            xco(J2,1)=x_1(i,1)+(step-1)*dx1;
      end;
end;

% REGION 2; segments 1 (N1+1) to N2 (N1+N2).
% Stepping over segments 1 to N2:
```

```
YY(2*fvar,2*fvar)=0;        % creation of (2 fvar)*(2 fvar) matrix YY.
for step=1:N2
        J1=N1*fvar+(step-1)*2*fvar;
        for i=1:p-1
                J2=(step-1)*(p-1)+i;
                J3=N1*(m-1)+J2;
                YY(:)=Y2(i,1:q);
                yy1(1:fvar,J3)=YY(1:fvar,1:2*fvar)*Ures(J1+1:J1+2*fvar,1);
                                                % FACE 1 solution vectors.

        yy2(1:fvar,J2)=YY(fvar+1:2*fvar,1:2*fvar)*Ures(J1+1:J1+2*fvar,1);
                                                % FACE 2 solution vectors.

                sc(J3,1)=Kz*yy1(2,J3);          % Found. transv. normal str.
                tc(J3,1)=-Kx2*0.5*tf1*yy1(3,J3); % Found. shear stress

                ssa(J2,1)=(Eaeff/ta)*(yy2(2,J2)-yy1(2,J3));
                                % Adhesive trans. normal stress (peel).
                tta(J2,1)=(Ga/ta)*(yy2(1,J2)-0.5*tf2*yy2(3,J2)-yy1(1,J3)-
                        0.5*tf1*yy1(3,J3));     % Adhesive shear stress.


                % Stress and moment resultants; FACE 1:
                Nx1(J3,1)=yy1(4,J3);    % Normal stress result.; FACE 1.
                Mx1(J3,1)=yy1(5,J3);    % Bending moment result.; FACE 1.
                Qx1(J3,1)=yy1(6,J3);    % Trans. shear str. result.; FACE 1.

                % Stress and moment resultants; FACE 2:
                Nx2(J2,1)=yy2(4,J2); % Normal stress result.; FACE 2.
                Mx2(J2,1)=yy2(5,J2); % Bending moment result.; FACE 2.
                Qx2(J2,1)=yy2(6,J2); % Trans. shear stress result.; FACE 2.

                xco(J3,1)=x_2(i,1)+L1+(step-1)*dx2;
        end;
end;

% Additional "arrangement" for last point in REGION 2, segment N2.
YY(:)=Y2(p,1:q);
yy1(1:fvar,J3+1)=YY(1:fvar,1:2*fvar)*Ures(J1+1:J1+2*fvar,1);
yy2(1:fvar,J2+1)=YY(fvar+1:2*fvar,1:2*fvar)*Ures(J1+1:J1+2*fvar,1);

sc(J3+1,1)=Kz*yy1(2,J3+1);                      % Found. transv. normal
                                                % stress.
tc(J3+1,1)=Kx2*(yy1(1,J3+1)+0.5*tf1*yy1(3,J3+1)); % Found. shear stress.

ssa(J2+1,1)=(Eaeff/ta)*(yy2(2,J2+1)-yy1(2,J3+1)); % Adhesive trans.
                                                % normal stress (peel).
tta(J2+1,1)=(Ga/ta)*(yy2(1,J2+1)+0.5*(tf2+ta)*yy2(3,J2+1)-
yy1(1,J3+1)+0.5*(tf1+ta)*yy1(3,J3+1));          % Adhesive shear
                                                % stress.
```

```
% Stress and moment resultants; FACE 1:
Nx1(J3+1,1)=yy1(4,J3+1);        % Normal stress resultant; FACE 1.
Mx1(J3+1,1)=yy1(5,J3+1);        % Bending moment resultant; FACE 1.
Qx1(J3+1,1)=yy1(6,J3+1);        % Trans. shear stress resultant; FACE 1.

% Stress and moment resultants; FACE 2:
Nx2(J2+1,1)=yy2(4,J2+1);        % Normal stress resultant; FACE 2.
Mx2(J2+1,1)=yy2(5,J2+1);        % Bending moment resultant; FACE 2.
Qx2(J2+1,1)=yy2(6,J2+1);        % Trans. shear stress resultant; FACE 2.

xco(J3+1,1)=L1+L2;

% Definition of "nominal" stress resultant Nnom, and "nominal" stress snom:
Nnom=Nx1(1);
snom=Nnom/tf1;
```

Appendix 11: STRAIN.m (calculation of strain components in the upper surfaces of the face-laminates; used by EXEC.m)

```
% M-file: STRAIN.m
%
% Calculation of surface strains in face-laminates 1 & 2.
% Creation of text-files epsX1.dat and epsX2.dat (ASCII-files)
% containing the calculated surface strains.

% REGION 1; segments 1 to N1.
% Stepping over segments 1 to N1:
for step=1:N1
  J1=(step-1)*fvar;
  for i=1:m-1
    J2=(step-1)*(m-1)+i;
    epsx1(J2,1)=Nx1(J2,1)/A1+(Mx1(J2,1)/Df1)*(tf1/2);
  end;
end;

% REGION 2; segments 1 (N1+1) to N2 (N1+N2).
% Stepping over segments 1 to N2:
for step=1:N2
  J1=N1*fvar+(step-1)*2*fvar;
  for i=1:p-1
    J2=(step-1)*(p-1)+i;
    J3=N1*(m-1)+J2;
    epsx1(J3,1)=Nx1(J3,1)/A1+(Mx1(J3,1)/Df1)*(tf1/2);
    epsx2(J2,1)=Nx2(J2,1)/A2+(Mx2(J2,1)/Df2)*(tf2/2);
  end;
end;

% Additional arrangement for last point in REGION 2,
```

```
% segment N2:
epsx1(J3+1,1)=Nx1(J3+1,1)/A1+(Mx1(J3+1,1)/Df1)*(tf1/2);
epsx2(J2+1,1)=Nx2(J2+1,1)/A2+(Mx2(J2+1,1)/Df2)*(tf2/2);

% CREATION OF output-file epsX1.dat and epsX2.dat
% containing the calculated surface strains:

OU=[xco epsx1];
fid=fopen('/t2/othomsen/TEXT/epsX1.dat','w');
fprintf(fid,'x      epsX1\n');
fprintf(fid,'%8.5f  %12.8f\n',OU');
status=fclose(fid);

OU=[xco2 epsx2];
fid=fopen('/t2/othomsen/TEXT/epsX2.dat','w');
fprintf(fid,'x2      epsX2\n');
fprintf(fid,'%8.5f  %12.8f\n',OU');
status=fclose(fid);
```

Appendix 12: TEXTout.m (creation of output text-files containing normalised adhesive/resin layer stresses, core stresses as well as face-laminate normalstress, bending moment and transverse shear stress resultants; used for graphical processing of results)

```
% M-file:  TEXTout.m
%
% Creation of output text-files (ASCII) containing the results of the analysis:
%  1a. w1out.dat:   lateral deflect.; face 1.
%  1b. w2out.dat:   lateral deflect.; face 2.
%  2.  adhes.dat:   adhesive stresses.
%  3.  found.dat:   foundation stresses.
%  4a. N1.dat:      Normal stress result. distrib.; face 1.
%  4b. N2.dat:      Normal stress result. distrib.; face 2.
%  5a. M1.dat:      Bending moment result. distrib.; face 1.
%  5b. M2.dat:      Bending moment result. distrib.; face 2.
%  6a. Q1.dat:      Trans. shear stress result. distrib.;face 1.
%  6b. Q2.dat:      Trans. shear stress result. distrib.;face 2.

OU=[xco w1];
fid=fopen('/t2/othomsen/TEXT/w1out.dat','w');
fprintf(fid,'x       w1\n');
fprintf(fid,'%8.5f  %12.8f\n',OU');
status=fclose(fid);

OU=[xco2 w2plot];
fid=fopen('/t2/othomsen/TEXT/w2out.dat','w');
```

```
fprintf(fid,'x2       "w2plot"\n');
fprintf(fid,'%8.5f  %12.8f\n',OU');
status=fclose(fid);

ssa=ssa/snom;       % Normalisation.
tta=tta/snom;       % Normalisation.
OU=[xco2 ssa tta];
fid=fopen('/t2/othomsen/TEXT/adhes.dat','w');
fprintf(fid,'x        ssa         tta\n');
fprintf(fid,'%8.5f  %12.8f  %12.8f\n',OU');
status=fclose(fid);

sc=sc/snom;         % Normalisation.
tc=tc/snom;         % Normalisation.
OU=[xco sc tc];
fid=fopen('/t2/othomsen/TEXT/found.dat','w');
fprintf(fid,'x         sc          tc\n');
fprintf(fid,'%8.5f  %12.8f  %12.8f\n',OU');
status=fclose(fid);

Nx1=Nx1/Nnom;    % Normalisation.
Nx2=Nx2/Nnom;    % Normalisation.
OU=[xco Nx1];
fid=fopen('/t2/othomsen/TEXT/N1.dat','w');
fprintf(fid,'x        Nx1\n');
fprintf(fid,'%8.5f  %12.8f\n',OU');
status=fclose(fid);

OU=[xco2 Nx2];
fid=fopen('/t2/othomsen/TEXT/N2.dat','w');
fprintf(fid,'x2       Nx2\n');
fprintf(fid,'%8.5f  %12.8f\n',OU');
status=fclose(fid);

OU=[xco Mx1];
fid=fopen('/t2/othomsen/TEXT/M1.dat','w');
fprintf(fid,'x        Mx1\n');
fprintf(fid,'%8.5f  %12.8f\n',OU');
status=fclose(fid);

OU=[xco2 Mx2];
fid=fopen('/t2/othomsen/TEXT/M2.dat','w');
fprintf(fid,'x2       Mx2\n');
fprintf(fid,'%8.5f  %12.8f\n',OU');
status=fclose(fid);

Qx1=Qx1/Nnom;    % Normalisation.
Qx2=Qx2/Nnom;    % Normalisation.
OU=[xco Qx1];
fid=fopen('/t2/othomsen/TEXT/Q1.dat','w');
fprintf(fid,'x        Qx1\n');
```

```
fprintf(fid,'%8.5f  %12.8f\n',OU');
status=fclose(fid);

OU=[xco2 Qx2];
fid=fopen('/t2/othomsen/TEXT/Q2.dat','w');
fprintf(fid,'x2        Qx2\n');
fprintf(fid,'%8.5f  %12.8f\n',OU');
status=fclose(fid);
```

Appendix 13: DEFORM.m (creation of line-plot showing the deformed structural configuration)

```
% M-file:  DEFORM.m
%
% Plot of deformed configuration.
% "Deflections" of the two face elements have been scaled.

plot(xco,w1,('r-'),xco2,w2plot,'g-.');
title('DEFORMED CONFIGURATION');
axis('off');
```

Appendix 14: DEFLECplot.m (creation of line-plot showing the lateral deflections of the face-laminates)

```
% M-file:  DEFLECplot.m
%
% Plot of lateral deflection of the two face elements.

plot(xco,w1,('r-'),xco2,w2,'g--');
title('LATERAL DEFLECTIONS');
xlabel('x-coordinate, [mm]');
ylabel('w1 (solid), w2 (dashed), [mm]');
```

Appendix 15: Adhestress.m (creation of line-plot showing the adhesive/resin stress distribution)

```
% M-file: Adhestress.m
%
% Plotting of adhesive layer stresses.
% The adhesive stresses are normalised with respect to the
% "nominal" stress snom.

ssa=ssa/snom;      % Normalisation.
tta=tta/snom;      % Normalisation.
```

```
plot(xco2,ssa,'r-',xco2,tta,'g--');
title('Normalised Adhesive layer peel and shear stress components');
xlabel('x2-coordinate, [mm]');
ylabel('ssa/snom (solid) & tta/snom (dashed)');
```

Appendix 16: Foundstress.m (creation of line-plot showing the core stress distribution)

```
% M-file: Foundstress.m
%
% Plotting of foundation stresses.
% The foundation stresses are normalised with respect  to the
% "nominal" stress snom.

sc=sc/snom;         % Normalisation.
tc=tc/snom;         % Normalisation.
plot(xco,sc,'r-',xco,tc,'g--');
title('Normalised foundation stress components');
xlabel('x-coordinate, [MPa]');
ylabel('sc/snom (solid) & tc/snom (dashed)');
```

Appendix 17: Ndistr.m (creation of line-plot showing the normal stress resultant distribution in the face-laminates)

```
% M-file: Ndistr.m
%
% Plotting of normal stress components.
% Nx1, Nx2 are normalised with respect to the "external load":
% Nx1(x=0)=Nnom.

Nx1=Nx1/Nnom;    % Normalisation.
Nx2=Nx2/Nnom;    % Normalisation.
plot(xco,Nx1,'r-',xco2,Nx2,'g--');
title('Normalised normal Stress Resultants: Nx1/Nnom and Nx2/Nnom');
xlabel('x-coordinate, [mm]');
ylabel('Nx1/Nnom (solid); Nx2/Nnom (dashed)');
```

Appendix 18: Mdistr.m (creation of lineplot showing the bending moment resultant distribution in the face-laminates)

```
% M-file: Mdistr.m
%
% Plotting of bending moment resultants: M1 & M2.
```

```
plot(xco,Mx1,'r-',xco2,Mx2,'g--');
title('Bending Moment Resultants: M1 and M2');
xlabel('x-coordinate, [mm]');
ylabel('Mx1,[N/mm] (solid); Mx2,[N/mm] (dashed)');
```

Appendix 19: Qdistr.m (creation of lineplot showing the transverse shear stress resultant distribution in the face-laminates)

```
% M-file: Qdistr.m
%
% Plotting of transverse shear stress resultants; Qx1, Qx2.
% Qx1, Qx2 are normalised with respect to the "external load":
% Nx1(x=0)=Nnom.

Qx1=Qx1/Nnom;    % Normalisation.
Qx2=Qx2/Nnom;    % Normalisation.
plot(xco,Qx1,'r-',xco2,Qx2,'g--');
title('Normalised Transverse Shear Stress Resultants: Q1/Nnom and
Q2/Nnom');
xlabel('x-coordinate, [mm]');
ylabel('Qx1/Nnom (solid); Qx2/Nnom (dashed)');
```

Appendix 20: STRAINplot.m (creation of lineplot showing the strain distribution in the upper surfaces of the face-laminates)

```
% M-file: STRAINplot.m
%
% Plotting of face-laminate surface-strains.

plot(xco,epsx1,'w-',xco2,epsx2,'g--');
title('Face-laminate surface strains: epsX1, epsX2');
xlabel('x-coordinate, [mm]');
ylabel('strain, [mm/mm]');
```